

BRIEF DEFINITIVE REPORT

Hepatic IRE1 α -XBP1 signaling promotes GDF15-mediated anorexia and body weight loss in chemotherapy

Yue Xiao Tang^{1,2*}, Tao Yao^{1,2,3*}, Xin Tian^{1,2,3}, Xintong Xia^{2,3}, Xingxiao Huang¹, Zhewen Qin¹, Zhong Shen⁴, Lin Zhao¹, Yaping Zhao⁵, Bowen Diao¹, Yan Ping¹, Xiaoxiao Zheng², Yonghao Xu¹, Hui Chen¹, Tao Qian⁶, Tao Ma⁶, Ben Zhou⁷, Suowen Xu⁵, Qimin Zhou⁸, Yong Liu⁹, Mengle Shao¹⁰, Wei Chen^{2,3}, Bo Shan¹¹, and Ying Wu^{2,3}

Platinum-based chemotherapy drugs can lead to the development of anorexia, a detrimental effect on the overall health of cancer patients. However, managing chemotherapy-induced anorexia and subsequent weight loss remains challenging due to limited effective therapeutic strategies. Growth differentiation factor 15 (GDF15) has recently gained significant attention in the context of chemotherapy-induced anorexia. Here, we report that hepatic GDF15 plays a crucial role in regulating body weight in response to chemo drugs cisplatin and doxorubicin. Cisplatin and doxorubicin treatments induce hepatic *Gdf15* expression and elevate circulating GDF15 levels, leading to hunger suppression and subsequent weight loss. Mechanistically, selective activation by chemotherapy of hepatic IRE1 α -XBP1 pathway of the unfolded protein response (UPR) upregulates *Gdf15* expression. Genetic and pharmacological inactivation of IRE1 α is sufficient to ameliorate chemotherapy-induced anorexia and body weight loss. These results identify hepatic IRE1 α as a molecular driver of GDF15-mediated anorexia and suggest that blocking IRE1 α RNase activity offers a therapeutic strategy to alleviate the adverse anorexia effects in chemotherapy.

Introduction

Platinum-based drugs are commonly used for cancer treatment, with cisplatin (Cis), carboplatin, and oxaliplatin as the most widely prescribed globally (Kelland, 2007). However, optimal use of this class of chemotherapy agents is restricted by dose-limiting side effects (Ruggiero et al., 2013), including nausea and emesis, anorexia, muscle wasting, and weight loss, which severely impact quality of life and limit treatment adherence. Despite almost 50 years of clinical use, mechanisms mediating these adverse effects associated with platinum-based therapies are yet to be fully understood, restraining effective strategies to overcome the undesired side effects. At present, much emphasis has been placed on alleviating nausea and emesis, and over

the last decade, substantial improvements in chemotherapy-induced nausea and vomiting control have been made with the current standard of care agents (5-hydroxytryptamine receptor [5-HT₃R] antagonists, neurokinin-1 receptor [NK-1] antagonists, dexamethasone, and olanzapine) (Hesketh et al., 2017). However, a significant percentage of individuals with cancer continue to have breakthrough or delayed emesis (Aapro et al., 2018; Einhorn et al., 2017; McCullough, 2017). Preclinical studies suggest that inhibition of nuclear factor κ -light-chain-enhancer of activated B cells and activin type 2 receptor signaling, or ghrelin receptor activation, could be beneficial for increasing body weight; however, the reported effects were modest

¹Zhejiang Provincial Key Laboratory of Pancreatic Disease, The First Affiliated Hospital, Institute of Translational Medicine, Zhejiang University School of Medicine, Zhejiang University, Hangzhou, China; ²Key Laboratory of Cancer Prevention and Therapy Combining Traditional Chinese and Western Medicine of Zhejiang Province, Zhejiang Academy of Traditional Chinese Medicine, Tongde Hospital of Zhejiang Province, Hangzhou, China; ³College of Life Sciences, Zhejiang Chinese Medical University, Hangzhou, China; ⁴Department of Coloproctology, Hangzhou Third People's Hospital, Hangzhou, China; ⁵Division of Life Sciences and Medicine, Department of Endocrinology, Institute of Endocrine and Metabolic Diseases, The First Affiliated Hospital of USTC, Clinical Research Hospital of Chinese Academy of Sciences (Hefei), University of Science and Technology of China, Hefei, China; ⁶Department of Hepatobiliary and Pancreatic Surgery, The First Affiliated Hospital, Zhejiang University School of Medicine, Hangzhou, China; ⁷CAS Key Laboratory of Nutrition, Metabolism and Food Safety, Shanghai Institute of Nutrition and Health, University of Chinese Academy of Sciences, Chinese Academy of Sciences, Shanghai, China; ⁸Department of Plastic and Reconstructive Surgery, Shanghai Ninth People's Hospital, Shanghai Jiao Tong University School of Medicine, Shanghai, China; ⁹Hubei Key Laboratory of Cell Homeostasis, College of Life Sciences, TaiKang Center for Life and Medical Sciences, Frontier Science Center for Immunology and Metabolism, The Institute for Advanced Studies, Wuhan University, Wuhan, China; ¹⁰CAS Key Laboratory of Molecular Virology and Immunology, The Center for Microbes, Development, and Health, Shanghai Institute of Immunity and Infection, Chinese Academy of Sciences, Shanghai, China; ¹¹Cancer Center, Zhejiang University, Hangzhou, China.

*Y. Tang and T. Yao contributed equally to this paper. Correspondence to Ying Wu: wuying@sibs.ac.cn; Bo Shan: boshan@zju.edu.cn; Wei Chen: viogro@163.com.

© 2024 Tang et al. This article is distributed under the terms of an Attribution–Noncommercial–Share Alike–No Mirror Sites license for the first six months after the publication date (see <http://www.rupress.org/terms/>). After six months it is available under a Creative Commons License (Attribution–Noncommercial–Share Alike 4.0 International license, as described at <https://creativecommons.org/licenses/by-nc-sa/4.0/>).

(Barreto et al., 2017; Chen et al., 2017; Peterson and Guttridge, 2008). Therefore, identification of new causal mechanism(s) of chemotherapy-induced body weight loss represents a critical step to inform novel strategies for optimizing platinum treatment and improving cancer care.

Growth differentiation factor 15 (GDF15) is a stress-responsive cytokine and a distant member of the transforming growth factor β superfamily (Bootcov et al., 1997; Breit et al., 2021; Tan et al., 2000; Tsai et al., 2018). GDF15 has been associated with numerous human diseases including cancer, cardiovascular disease, and inflammatory diseases (Breit et al., 2021; Tsai et al., 2018; Wang et al., 2021). Recently, a growing body of literature has documented the role of GDF15 in anorexia, weight loss, and cachexia in rodents and primates (Borner et al., 2020a, 2020b; Breen et al., 2020; Hsu et al., 2017; Wang et al., 2023). Evidence from rodents and shrews supports that GDF15 triggers anorexia through nausea and emesis, resulting in weight loss (Borner et al., 2020a). Notably, GDF15 levels are increased following administration of chemotherapy drugs (e.g., Cis, bleomycin, and doxorubicin [DOX]) (Breen et al., 2020). Increased GDF15 levels activate the glial cell-derived neurotrophic factor receptor α -like (GFRAL) whose expression is limited to the area postrema (AP) and the nucleus tractus solitarius (NTS) located in the hindbrain (Emmerson et al., 2017; Hsu et al., 2017; Mullican et al., 2017; Suriben et al., 2020). GDF15 administration increased c-Fos activation in AP/NTS, an area associated with cancer anorexia-cachexia syndrome in tumor-bearing animals in which plasma GDF15 levels are increased (Borner et al., 2020a; Hsu et al., 2017). Furthermore, antibody-mediated GDF15 neutralization alleviates chemotherapy-induced anorexia and weight loss in preclinical models (Breen et al., 2020), which implies a therapeutic potential in counteracting chemotherapy-associated side effects. Although the elevated circulating GDF15 and activation of GFRAL-expressing neurons localized in AP/NTS of the brainstem are accountable for chemotherapy-induced anorexia, it remains elusive that peripheral tissues or organs serve as the primary source of GDF15 and contribute to these adverse effects (Borner et al., 2020a; Breen et al., 2020; Hsu et al., 2017).

Originally characterized as a macrophage-secreted factor (Bootcov et al., 1997), the physiological expression of GDF15 is detected in liver, lung, kidney, and distal colon (Breen et al., 2020; Coll et al., 2020). Nevertheless, it appears that GDF15 is a general stress-induced cytokine in a wide variety of cell types (Appierto et al., 2009; Chung et al., 2017; Hsiao et al., 2000; Park et al., 2012; Patel et al., 2019; Yang et al., 2010), and regulation of *Gdf15* expression represents a critical mechanism by which serum GDF15 levels are controlled (Breen et al., 2020; Luan et al., 2019; Xie et al., 2022). However, due to its ubiquitous induction in response to various stimulations, regulatory mechanisms controlling *Gdf15* expression are highly diversified and context dependent (Breit et al., 2021; Tsai et al., 2018). For instance, the *Gdf15* transcription is actively regulated in injured and inflamed tissues and cells, and transcription factors including p53 (Tan et al., 2000) and Egr-1 (Baek et al., 2004) appear to be responsive for *Gdf15* induction in these settings (Wang et al., 2021). In a different context, transcriptional factors related to integrated

stress response emerge as critical regulators of *Gdf15* expression, which is induced in stress conditions or by drug treatments (Patel et al., 2019; Wang et al., 2021). Hence, as regulatory mechanisms of GDF15 production are heterogeneous, the full array of context-dependent transcriptional regulators has yet to be defined in the control of *Gdf15* expression.

Herein, we report that chemotherapy drugs acutely stimulate liver GDF15 production via selective activation of the hepatic ER stress sensor IRE1 α , an ER-resident transmembrane protein kinase/RNase that conveys a key signaling branch of the unfolded protein response (UPR) (Walter and Ron, 2011), thereby controlling the circulating GDF15 level. Genetic ablation of hepatic IRE1 α leads to reduced circulating GDF15, alleviating anorexia and body weight loss following chemotherapy drug treatments in tumor-bearing mice. Mechanistically, chemotherapy drugs activate hepatic IRE1 α RNase activity to produce the spliced active form of transcription factor XBP1, consequently promoting *Gdf15* expression in hepatocytes. In addition, pharmacological IRE1 α RNase inhibitor effectively suppresses liver *Gdf15* expression and circulating GDF15 levels, which is associated with improvements in chemotherapy-induced anorexia and body weight loss. Our findings thus unveil a stress-responsive mechanism underlying a liver-brain crosstalk that is pharmacologically targetable for alleviating the anorexic side effects associated with chemotherapy-induced body weight loss.

Results and discussion

Activation of hepatic UPR accompanies body weight loss upon chemotherapy

Documented studies have demonstrated that platinum-based chemotherapy (i.e., Cis) could cause body weight loss and anorexia in animals and subjects with cancers (Borner et al., 2020a; Breen et al., 2020; Hsu et al., 2017). To explore whether these side effects of chemotherapy are universal for other chemotherapy drugs, we administered 8-wk-old wild-type healthy mice with one dose of three main types of chemotherapeutic agents, Cis (platinum-based agent), DOX (anthracycline agent), and paclitaxel (PTX; taxane agent). In contrast to PTX, Cis and DOX treatment significantly repressed food intake at 1 day after injection and subsequently resulted in substantial body weight loss of the animals (Fig. S1, A and B), which is in agreement with previous studies (Breen et al., 2020). As liver is the central hub for drug metabolism in systemic administration of chemotherapeutic agents (Ramadori and Cameron, 2010; Tao et al., 2020), we reasoned that DOX and Cis treatment may exert profound impact on the liver. To this end, we employed bulk RNA sequencing (RNA-seq) to analyze the liver samples collected from mice at 1 day after DOX and Cis chemotherapy (Fig. 1 A). The sequencing data revealed extensive alterations in hepatic gene expression profiles from treated animals (Fig. 1, B and C). Whereas treatment by DOX and Cis elicited obviously different patterns of enriched pathways, the UPR appeared as a commonly upregulated pathway among the top 10 enriched pathways by Gene Set Enrichment Analysis (GSEA) of the two treatment groups (Fig. 1 D and Fig. S1, C–E). Notably, the analysis of significantly upregulated genes of the two treatment groups (823 in

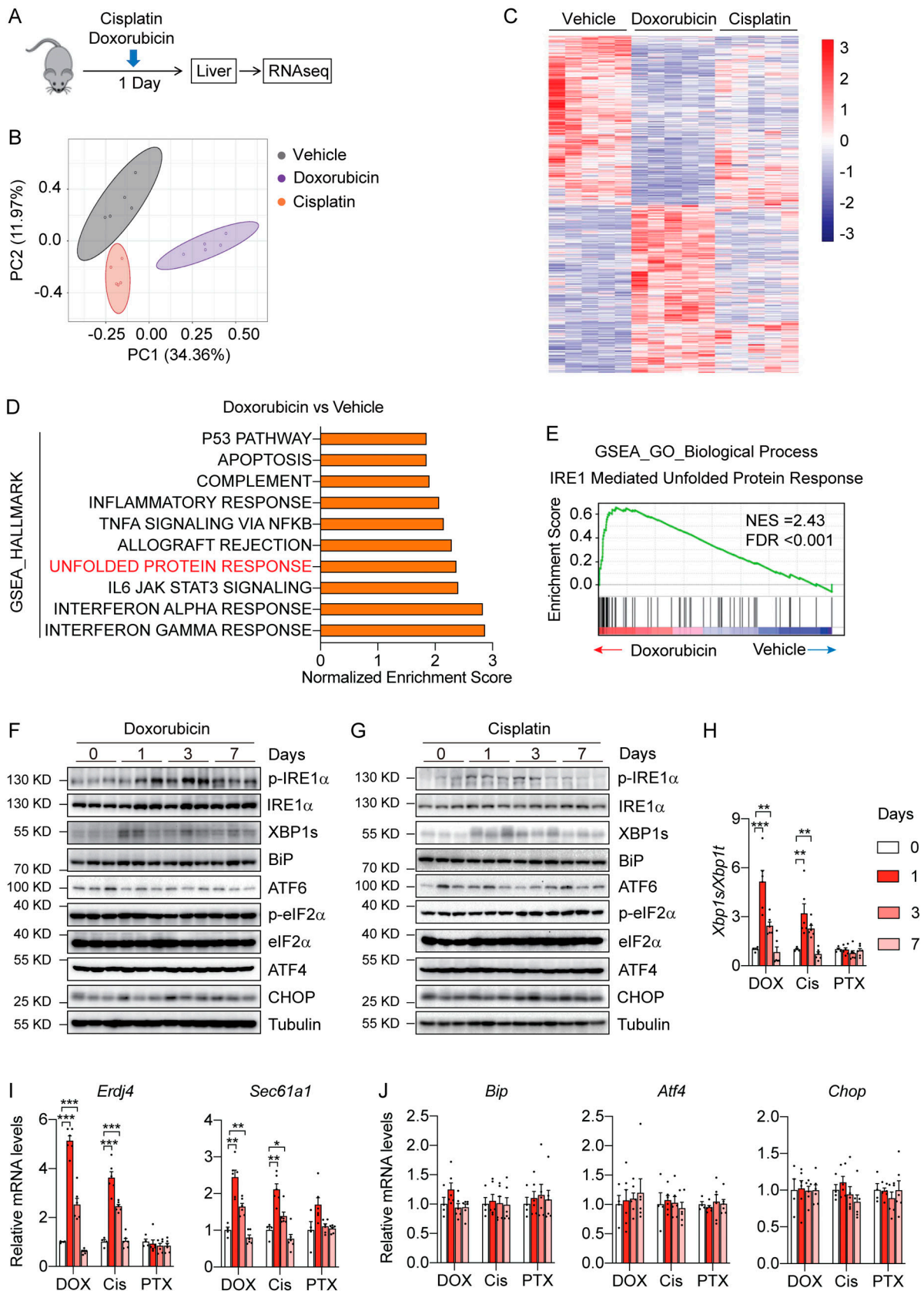


Figure 1. **Hepatic IRE1 α -XBP1 branch of the UPR is selectively activated by chemotherapy.** (A) Schematic illustration of the experimental design. 8-wk-old C57BL/6 male mice were treated with Vehicle ($n = 5$), a single dose of DOX (10 mg per kg body weight, i.p., $n = 5$), or Cis (10 mg per kg body weight, i.p., $n = 5$) for 1 day before liver samples were collected for bulk RNA-seq. (B) Principal component analysis of transcriptomic data obtained by bulk RNA-seq of liver

tissue from mice treated with Vehicle, DOX, or Cis for 1 day. **(C)** Heatmap visualization of the expression patterns of differentially expressed genes (DEGs) following chemotherapeutic drug administration. The cutoff values are $|\text{Log}_2(\text{Foldchange})| > 0.5$, and P value < 0.05 . For each group, the expression value is shown for five mice. **(D)** The top 10 enriched HALLMARK pathways by GSEA, which are differentially regulated in livers from Vehicle- and DOX-treated mice. HALLMARK pathways are defined using FPKM (fragments per kilobase million) values of all the detected genes in livers from DOX-treated mice and ranked according to NES. **(E)** GSEA plot indicating the enrichment (NES = 2.43 and FDR q-value < 0.001) of “IRE1-mediated unfolded protein response” gene signature in DOX-treated mice. The solid bars represent individual genes in this gene set. **(F and G)** 8-wk-old C57BL/6 male mice were treated with a single dose of (F) DOX (10 mg per kg body weight, i.p.) or (G) Cis (10 mg per kg body weight, i.p.). Liver samples were collected at indicated time (0, 1, 3, and 7 days) after injection. Western blot analysis showing the levels of the indicated proteins in liver lysates from the indicated mice. Each sample represents an individual animal. Tubulin was used as a loading control. **(H–J)** *Xbp1* mRNA splicing (H), mRNA levels of the indicated XBP1s target genes (I), and ER stress markers (J) in livers from mice treated with DOX (10 mg per kg body weight, i.p.), Cis (10 mg per kg body weight, i.p.), or PTX (10 mg per kg body weight, i.p.) for 0 ($n = 4$), 1 ($n = 6$), 3 ($n = 6$), and 7 days ($n = 6$). Data are representative of two independent experiments and presented as mean \pm SEM. * $P < 0.05$, ** $P < 0.01$, *** $P < 0.001$ by one-way ANOVA (H–J). Source data are available for this figure: SourceData F1.

DOX group and 216 genes in Cis group) revealed that the overlapping 135 transcripts are highly associated with the ER and involved in the response to ER stress according to Gene Ontology (GO) analysis (Fig. S1, F and H). These data indicate a link between hepatic UPR pathways and chemotherapy-associated anorexia and body weight loss.

The hepatic IRE1 α -XBP1 signaling pathway is selectively activated in mice upon chemotherapy

Given the diverse functions of the three UPR signaling branches in various physiological or pathological contexts (Hetz et al., 2020; Walter and Ron, 2011; Huang et al., 2019), we sought to determine which UPR branch(s) is/are activated in the liver upon chemotherapy. According to the GO Biological Process enrichment analysis, the “IRE1-mediated unfolded protein response” pathway is ranked (normalized enrichment score [NES] = 2.43 and false discovery rate [FDR] q-value < 0.001) in the top 10 pathways enriched in DOX-treated livers (Fig. 1 E and Fig. S1 I). Furthermore, MOTIF enrichment analysis revealed the activation of the IRE1 α -XBP1 branch, as evidenced by higher transcriptional activity of XBP1, a versatile transcription factor generated by IRE1 α -mediated unconventional mRNA splicing (Walter and Ron, 2011), in DOX-treated livers (Fig. S1, J and K). To further confirm this, we evaluated the activation of the three UPR pathways in the liver at different time intervals following DOX and Cis treatment. In line with the bioinformatics analysis, DOX- and Cis-treated mice displayed notably increased hepatic levels of phosphorylated IRE1 α and the spliced form of XBP1 (XBP1s) (Fig. 1, F and G; and Fig. S1, L and M) relative to their vehicle control counterparts. Additionally, enhanced *Xbp1* mRNA splicing as well as upregulated expression of XBP1s-target genes (*Erdj4*, *Sec61a1*) were also observed in the livers after 1-day chemotherapy (Fig. 1, H and I). However, neither the PERK-eIF2 α nor the ATF6 branches were apparently affected by chemotherapy, as evidenced by little changes in eIF2 α phosphorylation or the protein/mRNA abundance of BiP, CHOP, ATF4, and ATF6 (Fig. 1, F, G, and J; and Fig. S1, L and M). These results demonstrate that the hepatic IRE1 α -XBP1 signaling pathway is selectively activated in response to the treatment by chemotherapeutic drugs.

Loss of hepatic IRE1 α alleviates chemotherapy-induced anorexia and body weight loss

Notably, DOX and Cis could acutely exert its activating impact upon the IRE1 α -XBP1 pathway that peaked around 1 day after

injection (Fig. 1, F and G), coinciding with the instant body mass decline upon chemotherapy (Fig. S1, A and B). These observations prompted us to hypothesize that hepatic IRE1 α -XBP1 signaling may be directly involved in the development of chemotherapy-induced anorexia and body weight loss. To test this idea, we intercrossed *Ern1*^{flox/flox} mice, which harbor two loxP sites flanking the exon 2 of the *Ern1* gene (encoding IRE1 α protein), with *Albumin-Cre* transgenic mice (*Alb-Cre*) to generate hepatocyte-specific *Ern1* knockout mouse model (*Ern1*^{flox/flox}; *Alb-Cre*; denoted LKO) (Shao et al., 2014). Hepatic IRE1 α inactivation abolished the effects of DOX on inducing XBP1s protein accumulation, without affecting the other two UPR pathways in LKO livers (Fig. 2 A). Compared to their control counterparts, LKO mice showed remarkable improvements in food intake reduction and body weight loss induced by single or multiple doses of DOX treatments (Fig. 2, B and C). Moreover, hepatic IRE1 α ablation led to similar protection in the setting of Cis treatment (Fig. 2, D–F). These results demonstrate the critical role of hepatic IRE1 α in regulating anorexia and body weight loss in animals during chemotherapy.

To further determine whether hepatic IRE1 α exerts the same action in the development of chemotherapy-associated side effects under pathological conditions, we generated a tumor-bearing mouse model by subcutaneously implanting Hepa1-6 liver cancer cells in LKO and *flox/flox* control mice. Tumors were surgically removed from animals prior to DOX treatment, a process to mimic clinical chemotherapy received by cancer patients (Fig. 2 G). After the removal of visible tumors, the first dose of DOX injection caused the loss of body weight in both *flox/flox* and LKO mice (Fig. 2 H). However, the body weight of LKO mice recovered steadily and became indistinguishable from those of vehicle-treated control animals after two DOX injections, whereas the *flox/flox* group exhibited sustained body weight loss in response to the same treatment of DOX (Fig. 2 H). This affirms that hepatic IRE1 α exerts crucial actions in eliciting chemotherapy-induced body weight changes.

Liver-derived GDF15 mediates chemotherapy-induced anorexia and body weight loss

To explore how hepatic IRE1 α signaling pathway regulates anorexia and body weight loss during chemotherapy, we first analyzed genes whose expression was altered by chemotherapy drugs (Fig. 3 A). Among the 135 genes whose expression was commonly altered by Cis and DOX treatment, *Gdf15* exhibited a

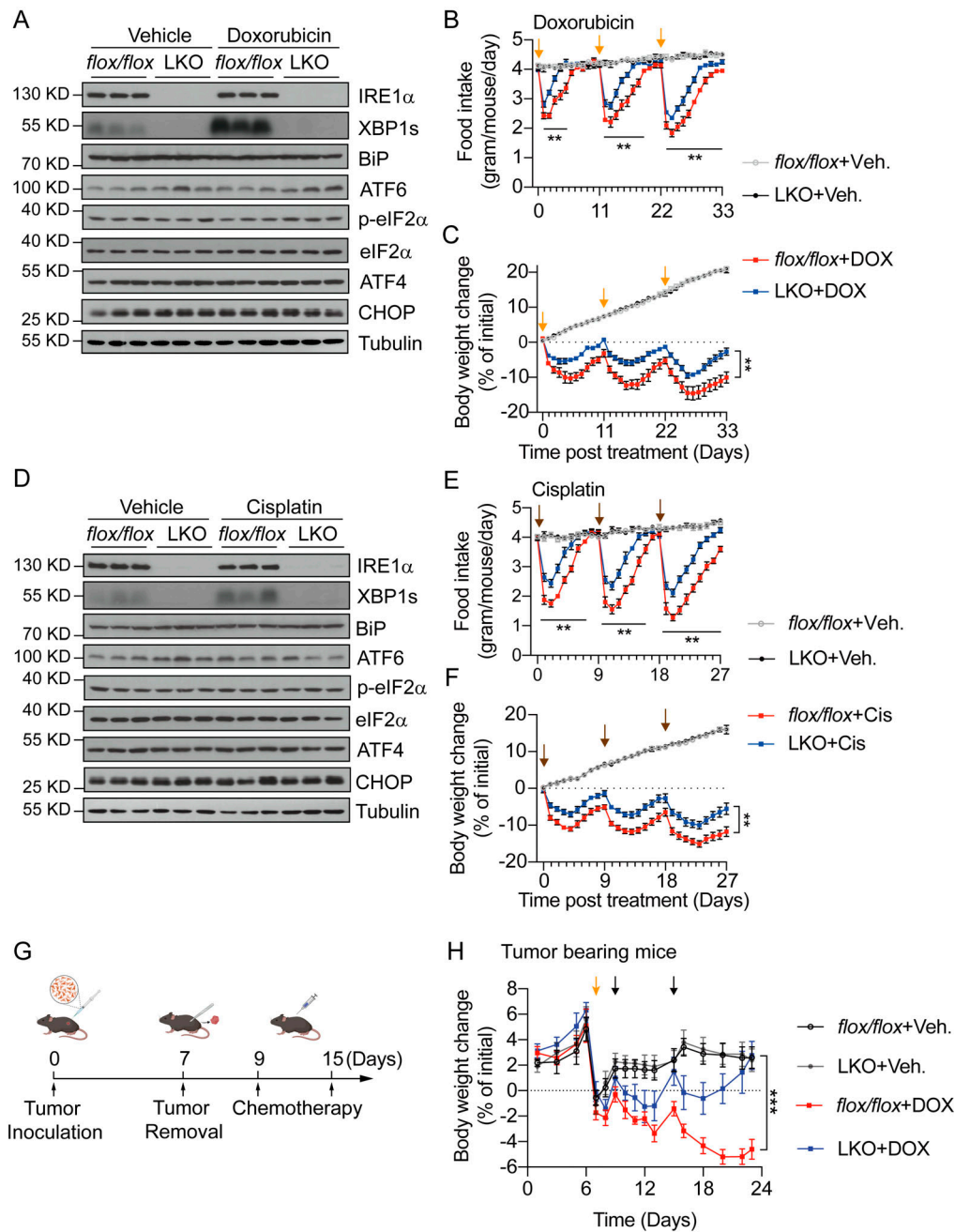


Figure 2. Hepatic IRE1 α ablation alleviates chemotherapy-induced anorexia and body weight loss. (A) Western blot analysis of the indicated proteins in liver lysates from *flox/flox* (*Ern1^{loxP/loxP}*, littermate controls) and LKO (*Ern1^{loxP/loxP}; Albumin-Cre*) mice treated with a single dose of Vehicle or DOX (5 mg per kg body weight, i.p.). Liver samples were collected 1 day after injection. Each sample represents an individual animal. Tubulin was used as a loading control. (B and C) Daily food intake (B) and body weight changes (C) of the indicated groups following Vehicle (Veh.) or DOX injection. *flox/flox+Veh.*, *n* = 6; LKO+Veh., *n* = 6; *flox/flox+DOX*, *n* = 6; LKO+DOX, *n* = 7. Yellow arrows indicate the time points of DOX injection (5 mg per kg body weight, i.p.). (D) Western blot analysis of the indicated proteins in liver lysates from *flox/flox* and LKO mice treated with a single dose of Vehicle or Cis (5 mg per kg body weight, i.p.). Liver samples were collected 1 day after injection. Each sample represents an individual animal. Tubulin was used as a loading control. (E and F) Daily food intake (E) and body weight changes (F) of the indicated groups following Vehicle (Veh.) or Cis injection. *flox/flox+Veh.*, *n* = 6; LKO+Veh., *n* = 6; *flox/flox+Cis*, *n* = 8; LKO+Cis, *n* = 7. Brown arrows indicate the time points of Cis injection (5 mg per kg body weight, i.p.). (G) Schematic illustration of the experimental design. 8-wk-old male *flox/flox* and LKO mice were subcutaneously inoculated with Hepa1-6 cells to induce tumor formation. DOX (5 mg per kg body weight) or Vehicle was i.p. administered, and visible tumors were removed by surgery at the indicated time. (H) Body weight changes in tumor-bearing and -resected *flox/flox* and LKO mice treated with Vehicle or DOX. *flox/flox+Veh.*, *n* = 10; LKO+Veh., *n* = 8; *flox/flox+DOX*, *n* = 12; LKO+DOX, *n* = 10. Yellow arrow indicates the time point of tumor removal. Black arrows indicate the time points of DOX or Vehicle treatment. Data are representative of two independent experiments and presented as mean \pm SEM. ***P* < 0.01, or ****P* < 0.001 by unpaired two-tailed Student's *t* test (B, C, E, F, and H). Source data are available for this figure: SourceData F2.

most prominent upregulation, and it top-ranked among the 26 genes encoding putative secretory factors, according to the RNA-seq datasets (Fig. 3 B). In line with its anorexic effects, treatment by both DOX and Cis, but not by PTX, led to robust elevation of hepatic *Gdf15* mRNA levels and circulating GDF15 protein abundance in mice (Fig. 3, C and D). In human patients, remarkably, circulating levels of GDF15 were also dramatically elevated in colon cancer and breast cancer individuals after receiving the first dose of chemotherapy (Fig. 3 E). To confirm the necessity and sufficiency of GDF15 for chemo-induced anorexia, we employed whole-body *Gdf15* gene knockout mouse model (*Gdf15*^{KO}). Compared to their control counterparts, *Gdf15*^{KO} mice showed marked improvements in food intake reduction and body weight loss upon DOX or Cis treatment (Fig. S2, A-H). Emerging evidence has shown that GDF15 is a stress-induced hepatokine and acts as a pivotal mediator in regulating chemotherapy-induced anorexia and body weight loss via its obligate receptor GFRAL expressed in neurons localized in AP/NTS of the brainstem (Borner et al., 2020a; Breen et al., 2020; Hsu et al., 2017; Luan et al., 2019). Therefore, we next asked whether liver-derived GDF15 serves as a major contributor to its elevated circulating levels upon chemotherapy. We first assessed *Gdf15* mRNA levels in various tissues/organs and found that the liver displayed the most robust expression and upregulation of *Gdf15* mRNA in response to both DOX and Cis treatments (Fig. 3 F). Then, we employed adenovirus-associated virus to deliver *Gdf15*-targeting shRNA (AAV-sh*Gdf15*) to knock down the expression of *Gdf15* specifically in the liver (Cunningham and Alexander, 2019) (Fig. S2, I and J). AAV-sh*Gdf15* significantly reduced hepatic *Gdf15* mRNA induction and subsequently the elevation of circulating GDF15 levels in mice following Cis administration (Fig. 3, G and H). Consistently, mice injected with AAV-sh*Gdf15* exhibited significant improvements in anorexia and body weight loss relative to animals injected with control viruses after the same dose of Cis treatment (Fig. 3, I and J). These results indicate that in the context of chemotherapy, liver-derived GDF15 is a key factor that drives the development of anorexia and body weight loss.

Hepatic IRE1 α -XBP1s pathway controls chemotherapy-induced GDF15 expression

Because the induction of hepatic *Gdf15* expression (Fig. 3, C and F) concurs with the activation of the IRE1 α -XBP1s signaling pathway during chemotherapy (Fig. 1, F-I; and Fig. S2 K), we asked whether IRE1 α -XBP1s signaling is involved in mediating chemotherapy-induced *Gdf15* expression in the liver. To test this, we overexpressed IRE1 α or XBP1s in human hepatoma Huh7 cells, which led to a robust increase in *GDF15* expression (Fig. 4, A and B). Conversely, silencing the expression of *ERN1* (the gene encoding human IRE1 α) by si-*ERN1* efficiently blunted the inducing effects of chemotherapy drugs on *GDF15* expression (Fig. 4 C and Fig. S2, L and M). We then tested whether *Gdf15* is a direct transcriptional target of the IRE1 α -XBP1 pathway. To this end, we engineered a reporter construct in which the expression of luciferase is driven by the promoter portion at 1,028 bp upstream of murine *Gdf15* gene transcription start site. Notably, a putative ER stress-response element (ERSE) was identified

within this region (Fig. 4 D) (Yamamoto et al., 2004). Luciferase reporter assays showed that XBP1s directly stimulated the *Gdf15* promoter activity, which was abolished by mutation of the putative ERSE (Fig. 4 D). Furthermore, we performed chromatin immunoprecipitation (ChIP) assays, using nuclear extracts from primary hepatocytes overexpressing GFP or XBP1s. Indeed, XBP1s could bind to the putative ERSE-containing region of the *Gdf15* promoter (Fig. 4 E). Moreover, imaging analyses of mice with engineered *Gdf15* promoter-Luc reporter in their livers showed that hepatocyte-specific deletion of IRE1 α attenuated chemotherapy-induced activation of the *Gdf15* promoter in vivo (Fig. 4 F). Thus, these data demonstrate that XBP1s directly binds to and activates *Gdf15* promoter, suggesting that chemotherapy-activated liver IRE1 α -XBP1 pathway acts through a transcriptional regulatory mechanism for the associated increase of GDF15 levels and the consequential anorexia.

Then, we evaluated the effect of hepatic IRE1 α deficiency upon *Gdf15* expression and circulating GDF15 levels in LKO mice in vivo. In parallel with the suppression of *Xbp1* mRNA splicing (Fig. 4 G), genetic ablation of liver IRE1 α markedly attenuated DOX-induced upregulation of hepatic *Gdf15* mRNA expression (Fig. 4 H) and serum GDF15 protein level (Fig. 4 I) relative to that in control animals. Moreover, serum GDF15 levels in tumor-bearing LKO mice were significantly reduced to ~55% of those in control animals after DOX administration (Fig. 4 J). Reported studies have demonstrated that anorexia in chemotherapy can be ascribed to elevated circulating levels of GDF15, which activates c-Fos in GFRAL-expressing neurons localized to AP/NTS of the brainstem (Borner et al., 2020a; Breen et al., 2020; Hsu et al., 2017). In agreement, relative to control animals, the decline of circulating GDF15 protein levels in DOX-treated LKO mice was paralleled with lower abundance of GFRAL⁺c-Fos⁺ neurons in AP (Fig. 4 K). Similar effects were also observed in Cis-treated LKO mice (Fig. 4, L-O). Notably, deficiency of hepatic IRE1 α did not exert detectable effects on liver homeostasis or chemo-induced hepatic damages (Fig. S3, A-F). Together, these results support a key role of hepatic IRE1 α -XBP1s-GDF15 axis in promoting the development of anorexia during chemotherapy.

Pharmacologic blocking of IRE1 α RNase alleviates chemotherapy-induced anorexia and body weight loss

Considering the in vitro and in vivo evidence showing the regulation by hepatic IRE1 α -XBP1 pathway of chemotherapy-induced GDF15 production in body weight loss, we further examined whether pharmacologic inhibition of IRE1 α could effectively alleviate these side effects. Indeed, treatment with 4 μ 8C, a chemical inhibitor of IRE1 α RNase activity, substantially suppressed the induction of GDF15 in both DOX- and Cis-treated Huh7 cells (Fig. 5, A and B). Then, we determined whether chemotherapy-induced anorexia and body weight loss could be corrected through such pharmacologic blocking of IRE1 α RNase activity in vivo. To this end, we administered mice with 4 μ 8C in combination with DOX and observed apparent suppression of *Xbp1* mRNA splicing in the liver, indicating that hepatic IRE1 α RNase activity could be efficiently inhibited by 4 μ 8C treatment (Fig. 5 C). Consistently, 4 μ 8C treatment robustly decreased hepatic *Gdf15* mRNA expression and lowered serum GDF15 levels in

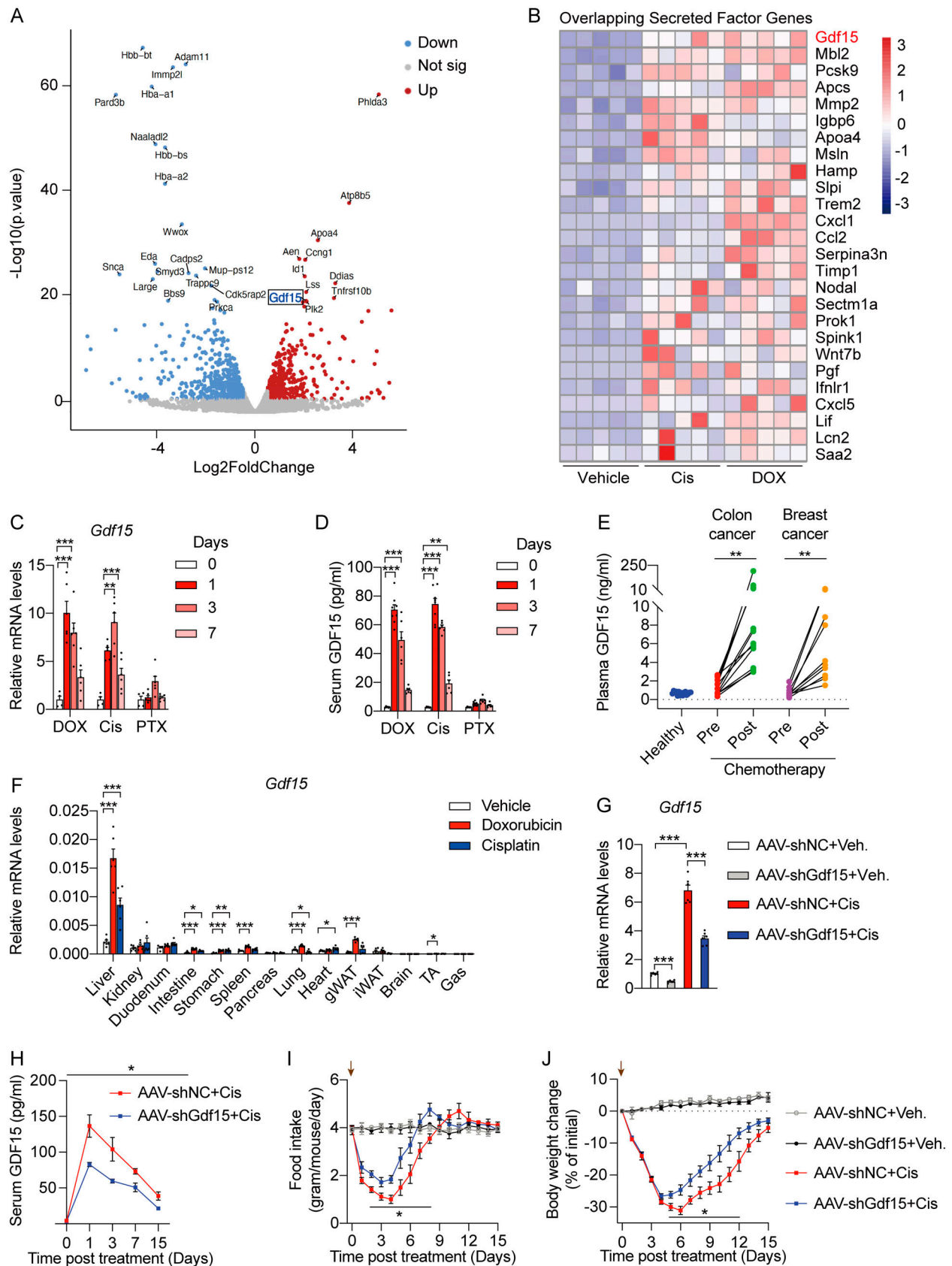


Figure 3. **Liver-derived GDF15 mediates chemotherapy-induced anorexia and body weight loss.** (A) Volcano plot showing DEGs (FDR < 0.05 and $|\text{Log}_2(\text{Foldchange})| > 2$) between the liver samples from Vehicle- and Cis-treated mice. Significantly changed genes are colored in red (upregulated, Up) and blue (downregulated, Down), while non-significantly changed genes (Not sig) are in gray. (B) Heatmap of 26 genes encoding secreted factors among 135 overlapping

upregulated genes (compared to Vehicle treatment) in liver samples from both DOX- and Cis-treated mice. **(C and D)** mRNA levels of *Gdf15* in livers (C) and circulating GDF15 protein levels (D) from mice treated with the indicated chemotherapy drugs (DOX, 10 mg per kg body weight, i.p.; Cis, 10 mg per kg body weight, i.p.; or PTX, 10 mg per kg body weight, i.p.) for 0 ($n = 4$), 1 ($n = 6$), 3 ($n = 6$), and 7 days ($n = 6$). **(E)** Circulating GDF15 protein levels in healthy volunteers (non-tumor) and in individuals with colon or breast cancer before and after receiving chemotherapy for the first time (healthy volunteer, $n = 15$; colon cancer patients, $n = 12$; breast cancer patients, $n = 10$). **(F)** mRNA levels of *Gdf15* in various tissues isolated from mice treated with Vehicle ($n = 6$), DOX ($n = 6$), or Cis ($n = 6$). Tissues were collected 1 day after injection. gWAT, gonadal white adipose tissue; iWAT, inguinal white adipose tissue; TA, tibialis anterior; Gas, gastrocnemius. **(G–J)** C57BL/6 male mice were injected with AAV-shNC ($n = 12$) or AAV-shGdf15-1 ($n = 12$) for 4 wk before i.p. injection of Cis (10 mg per kg body weight) or Vehicle. **(G and H)** Liver *Gdf15* mRNA abundance (G) and circulating GDF15 protein levels (H) were quantified in liver samples collected 1 day after injection and serum samples harvested at the indicated time points following Cis treatment, respectively. AAV-shNC+Veh., $n = 6$; AAV-shGdf15+Veh., $n = 6$; AAV-shNC+Cis, $n = 6$; AAV-shGdf15+Cis, $n = 6$. **(I and J)** Daily food intake (I) and body weight changes (J) of AAV-shNC- and AAV-shGdf15-injected mice following Vehicle or Cis treatment. The arrow indicates the time point of Cis injection. Data are representative of two independent (except A, B, and E) experiments and presented as mean \pm SEM. * $P < 0.05$, ** $P < 0.01$, or *** $P < 0.001$ by one-way ANOVA (C, D, and F), two-way ANOVA (G), unpaired two-tailed Student's *t* test (H–J), or paired Student's *t* test (E).

DOX-treated mice (Fig. 5, D and E). Notably, a decreased number of GFRAL⁺c-Fos⁺ neurons in AP was also observed in mice treated with DOX plus 4 μ 8C (Fig. 5 F). As expected, 4 μ 8C treatment markedly dampened the development of anorexia and body weight loss upon chemotherapy in animals (Fig. 5, G and H). In addition, administration of 4 μ 8C in Cis-treated mice resulted in similar phenotypic effects, i.e., reduced GDF15 induction and alleviated body weight loss (Fig. 5, I–N). Notably, 4 μ 8C treatment did not exert noticeable effects upon liver homeostasis or chemo-induced hepatic damages (Fig. S3, G–L). Together, these data demonstrate that pharmacologic inhibition of IRE1 α RNase activity can effectively alleviate chemotherapy-associated anorexia and body weight loss.

Concluding remarks

As the main chemotherapy drugs used in clinical treatment of solid tumors, platinum-based chemotherapeutic agents such as Cis as well as DOX can cause nausea, vomiting, and anorexia, resulting in body weight loss and poor life quality in the patients. Approximately half of the patients undergoing chemotherapy suffer from chemotherapy-induced anorexia (Hong et al., 2006; Winton et al., 2005). Owing to the largely elusive mechanisms underlying these adverse effects, there are limited therapeutic strategies for effective treatment. Documented studies have revealed that Cis treatment leads to excessive serotonin (5-HT) release from the gastrointestinal tract into circulation followed by abnormal dynamics of an hunger-stimulating hormone ghrelin, which may directly stimulate 5-HT receptors in the postrema area of the central nervous system (Minami et al., 2003). Although application of antagonists for 5-HT_{3R} and NK-1 receptor has been shown to improve chemotherapy-induced nausea, breakthrough or delayed emesis could still be observed in a significant percentage of individuals with cancers (Aapro et al., 2018; Einhorn et al., 2017; McCullough, 2017). Recently, a critical role of the GDF15-GFRAL axis has been uncovered in regulating the occurrence of chemotherapy-induced nausea, anorexia, and weight loss in rodents, shrews, and primates (Borner et al., 2020a, 2020b; Breen et al., 2020; Hsu et al., 2017). Elevation of circulating GDF15 levels and activation of the GFRAL neurons in the postrema area of hindbrain were observed in animals treated with platinum-based drugs. Importantly, inhibition of the GDF15-GFRAL axis by neutralizing circulating GDF15 protein with monoclonal antibodies or by ablating *Gfral* gene profoundly

alleviated anorexia and weight loss during platinum-based chemotherapy (Breen et al., 2020; Hsu et al., 2017). Here, our results demonstrate that treatment with DOX, another chemotherapy agent with high clinical emetic scores, can also robustly elevate circulating GDF15 levels along with anorexia and body weight loss in both healthy and tumor-bearing animals, in contrast to PTX, which has low clinical emetic scores. This is in line with previous studies regarding platinum-based drugs (Breen et al., 2020). Importantly, we observed elevated levels of plasma GDF15 not only in animal studies, but also in individuals with colon or breast cancers receiving the first dose of platinum-based or DOX-based chemo drugs (Fig. 3 E). These effects are much more dramatic than the results observed in a previous study involving patients who underwent multiple rounds of undefined chemotherapy. This suggests a significant and immediate response of GDF15 expression to chemotherapy treatment.

Our results from animal models showed that liver-derived GDF15 critically mediates chemotherapy-induced anorexia and body weight loss, supporting its role as an endocrine factor in the liver-brain communication via neural circuitry (Matsubara et al., 2022). A number of hepatocyte-derived secreted factors, namely “hepatokines,” have been documented as essential information transmitters that sense liver metabolic status and regulate systemic metabolism through target organs such as the brain, such as FGF21 and GDF15 (Jensen-Cody and Potthoff, 2021). In response to starvation and stress conditions, hepatocyte-derived FGF21 acts as an endocrine hormone to regulate a variety of physiological aspects including glucose/lipid metabolism, energy expenditure, and insulin/leptin sensitivity (Hill et al., 2019; Maida et al., 2016; Potthoff et al., 2009). Recent studies have also highlighted FGF21 signaling in the control of carbohydrate intake and taste preference through glutamatergic neurons in mice (von Holstein-Rathlou et al., 2016). Likewise, GDF15 acts through its obligate receptor GFRAL, whose expression is strictly limited to hindbrain, a critical area for the physiological control of emesis, nausea, and vomiting (Borner et al., 2020a). Notably, GDF15 is also a ubiquitous stress-responsive endocrine factor, whose expression has been shown to be regulated by integrated stress response transcription factors ATF4 and CHOP (Day et al., 2019; Miyake et al., 2021; Xie et al., 2022). With a lower hepatic expression under basal conditions, liver-secreted GDF15 exerts its metabolic actions in the settings where its expression is induced by stress, injury, or

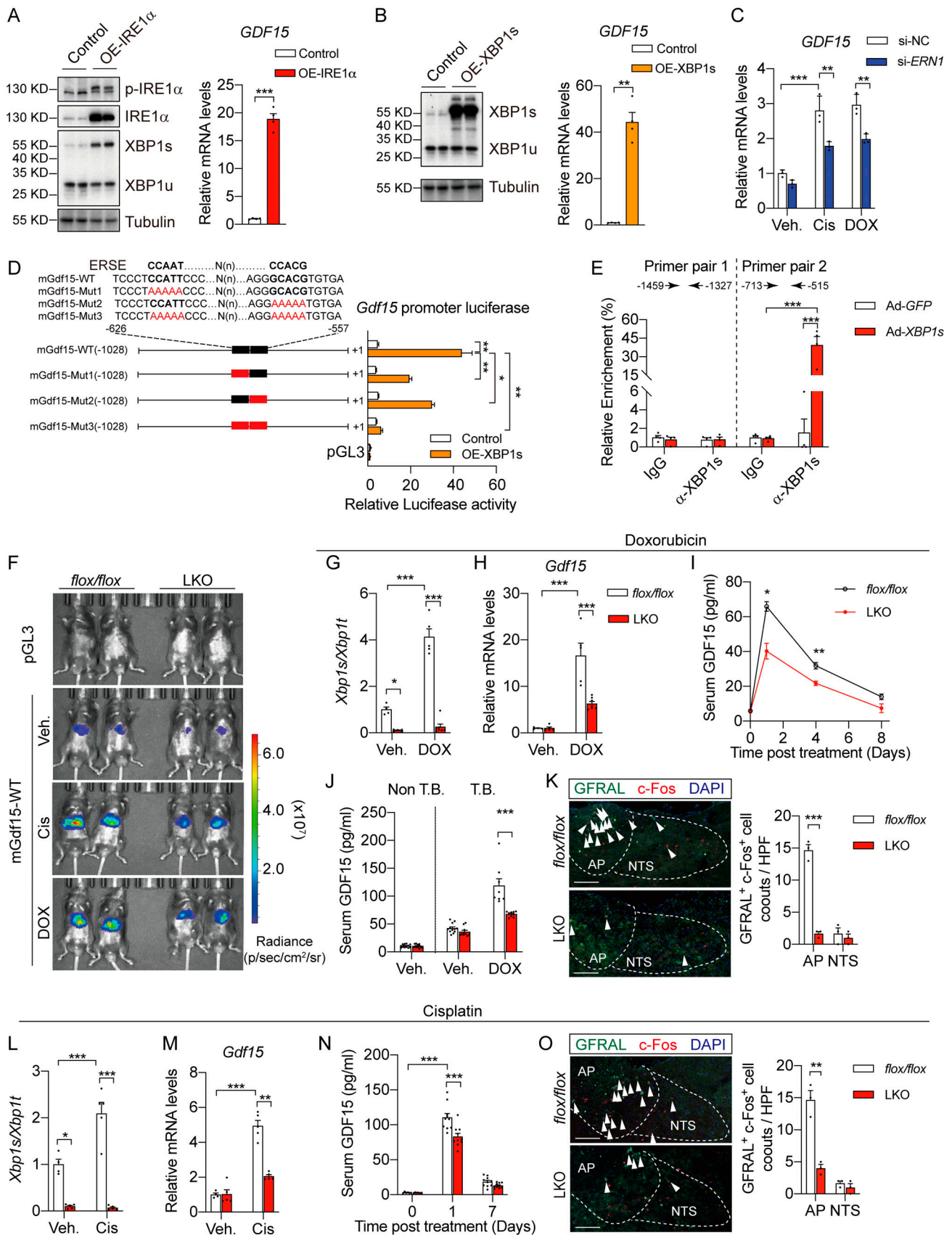


Figure 4. **The IRE1 α -XBP1 pathway mediates chemotherapy-induced hepatic GDF15 upregulation.** (A and B) Western blot analysis of the indicated proteins (left) and RT-qPCR analysis of *GDF15* mRNA abundance (right) in cell lysates of Huh7 cells transfected with control vector, or vector expressing IRE1 α

(OE-IRE1 α) (A) or XBP1s (OE-XBP1s) (B). Tubulin was used as a loading control. (C) *Gdf15* mRNA levels in Huh7 cells transfected with control siRNA (si-NC) or *ERN1* knockdown siRNA (si-*ERN1*) prior to treatment with DOX (0.01 μ g/ml) or Cis (10 μ M) for 48 h. $n = 3$ per group. (D) Schematic of the luciferase constructs of *Gdf15* promoter with the ERSE-like sequence indicated. Luciferase reporter assays were performed by co-transfection of HEK293T cells with the control vector or pCMV-XBP1s plasmid together with Luc constructs under the control of the mouse *Gdf15* promoter (WT) or those with mutant ERSE sequences (Mut1, Mut2, Mut3). $n = 3$ per group. (E) ChIP-qPCR analysis of XBP1s binding site on *Gdf15* promoter was performed by overexpression of XBP1s in primary hepatocytes ($n = 4$). ChIP-qPCR of the segments containing XBP1s-binding site (-713 to -515) or no XBP1s-binding site (-1,459 to -1,327) within the *Gdf15* promoter. (F) *flox/flox* (littermates) and LKO mice were engineered to express the empty control construct or the *Gdf15*-WT Luc reporter in livers. Luciferase activities were monitored in vivo by the imaging system under the indicated treatments. Mice were i.p. administered with DOX (5 mg per kg body weight) or Cis (5 mg per kg body weight) 24 h prior to luciferase assays. (G and H) *Xbp1* mRNA splicing (G) and mRNA levels of *Gdf15* (H) in livers from *flox/flox* and LKO mice following DOX treatment (5 mg per kg body weight, i.p.) for 1 day. *flox/flox*+Veh., $n = 4$; LKO+Veh., $n = 5$; *flox/flox*+DOX, $n = 5$; LKO+DOX, $n = 7$. (I) Circulating GDF15 protein levels in *flox/flox* ($n = 7$) and LKO ($n = 7$) mice at the indicated time points following DOX treatment (5 mg per kg body weight, i.p.). (J) Serum GDF15 protein levels in non-tumor-bearing (Non T.B.) *flox/flox* ($n = 12$) and LKO ($n = 12$) mice, and in tumor-bearing (T.B.) *flox/flox* and LKO mice treated with Vehicle (Veh.; $n = 12$ for *flox/flox*, $n = 10$ for LKO) or DOX (5 mg per kg body weight, i.p., $n = 12$ for each group) for 1 day. (K) Representative images of immunofluorescence staining against c-Fos and GFRAL at the AP and NTS of the murine brainstem (left). GFRAL⁺ c-Fos⁺ cells (indicated by arrowheads, left) in AP or NTS per high power field (HPF) were quantified (right). The frozen brainstem slides were from *flox/flox* and LKO mice at 1 day after DOX treatment (5 mg per kg body weight, i.p.). Scale bar, 100 μ m. (L and M) *Xbp1* mRNA splicing (L) and mRNA levels of *Gdf15* (M) in liver samples from *flox/flox* and LKO mice following Cis treatment (5 mg per kg body weight, i.p.) for 1 day. *flox/flox*+Veh., $n = 4$; LKO+Veh., $n = 5$; *flox/flox*+Cis, $n = 5$; LKO+Cis, $n = 5$. (N) Circulating GDF15 protein levels in *flox/flox* ($n = 10$) and LKO ($n = 10$) mice at the indicated time points following Cis treatment (5 mg per kg body weight, i.p.). (O) Representative images of immunofluorescence staining against c-Fos and GFRAL at the area AP and NTS of the murine brainstem (left). GFRAL⁺ c-Fos⁺ cells (indicated by arrowheads, left) per HPF were quantified (right). The frozen brainstem slides were from *flox/flox* and LKO mice at 1 day after Cis treatment (5 mg per kg body weight, i.p.). Scale bar, 100 μ m. Data are representative of three independent experiments (A–G) or two independent experiments (H–P) and presented as mean \pm SEM. * $P < 0.05$, ** $P < 0.01$, or *** $P < 0.001$ by unpaired two-tailed Student's *t* test (A, B, I, K, and O) or two-way ANOVA (C–H, J, L–N). Source data are available for this figure: SourceData F4.

drug administration (Patel et al., 2022). While GDF15's cellular origin is highly diversified (Patel et al., 2019), the physiological and pathological significance of hepatic GDF15 production has remained obscure in various contexts. An intriguing observation in our study is that mice in some cohorts displayed rapid normalization of food intake, but with relatively slow regaining of body weight during the recovery phase after chemotherapy challenge, similar to patterns as previously documented (Borner et al., 2020a). This delayed regaining of body weight may stem from several factors, such as delayed systemic storage of assimilated energy and nutrients, other chemotherapy-induced, metabolically adverse effects, or multiple metabolic actions of GDF15, e.g., promoting adipose tissue lipolysis for lipid utilization and energy production (Suriben et al., 2020; Hsu et al., 2017; Wang et al., 2023).

In the current study, we have found that the IRE1 α -XBP1 branch of the UPR is selectively activated, which subsequently upregulates the expression of *Gdf15* gene in the liver upon DOX or Cis treatments. This unveils an ER stress-mediated mechanism that links elevated liver GDF15 production to chemotherapy drug-induced adverse effects. IRE1 α has been established as a key metabolic stress sensor and regulator of liver metabolism in response to nutritional states and various stimuli, including fasting/refeeding conditions and many endocrine factors (Huang et al., 2019). Here, our results reveal that chemotherapy drugs can also selectively activate the IRE1 α -XBP1 pathway in hepatocytes, but not the PERK or ATF6 branches of UPR (Fig. 1). With respect to their mechanisms of action, Cis is known to form DNA crosslinks, blocking DNA, and RNA synthesis (Dasari and Tchounwou, 2014), and DOX can intercalate DNA, inhibiting topoisomerase II and RNA polymerase II activity and inducing DNA damage (Minotti et al., 2004), whereas PTX may prevent microtubule depolymerization, blocking the G2/M phase of cell division (Jordan and Wilson, 2004). Thus, it remains to be deciphered how the DNA-damaging chemotherapeutic agents can

selectively trigger the activation of the IRE1 α -XBP1 pathway in the liver.

It is particularly worth noting that hepatic *Gdf15* expression is under the control of XBP1s, suggesting a potential therapeutic opportunity to target liver IRE1 α RNase activity for ameliorating chemotherapy-induced anorexic effects. Targeting the signaling molecules of the UPR to combat various diseases has gained an increasing attraction in recent years (Marciniak et al., 2022). An array of compounds or drug-like molecules targeting the UPR sensors such as IRE1 α has become available and is being tested in clinical trials (Marciniak et al., 2022). For instance, two clinical trials for the chemical compound ORIN1001, a specific inhibitor of IRE1 α RNase activity, have been under way in patients with advanced solid tumors (NCT05154201, NCT03950570). Given that IRE1 α also serves as a therapeutic target in tumor therapy, our results may point to an additional therapeutic benefit since selective blocking of hepatic IRE1 α RNase activity is effective in reducing chemotherapy-induced GDF15 production to ameliorate GDF15-dependent anorexic side effects. It is also noteworthy that both DOX and Cis could still induce slight reductions of food intake and body weight in *Gdf15*^{KO} mice (Fig. S2, A–H). Besides GDF15, our results also revealed ~25 secreted factors whose expression increased in response to both chemo drugs (Fig. 3 B). Therefore, it warrants further investigations to explore additional mechanisms by which hepatic IRE1 α -XBP1s signaling pathway mediates the adverse effects of chemotherapy beyond its regulation of GDF15 production in the context of not only anorexia, but also nausea and malaise as well as other possible behavioral changes. It would be also of great translational significance to dissect whether targeting the IRE1 α pathway can be more efficacious than modulating the GDF15-GFRAL axis in these settings.

In summary, our study demonstrates that IRE1 α -dependent upregulation of hepatic *Gdf15* expression serves as a key mechanism driving chemotherapy-associated anorexia and body weight loss. Upon chemotherapy, selective activation of hepatic

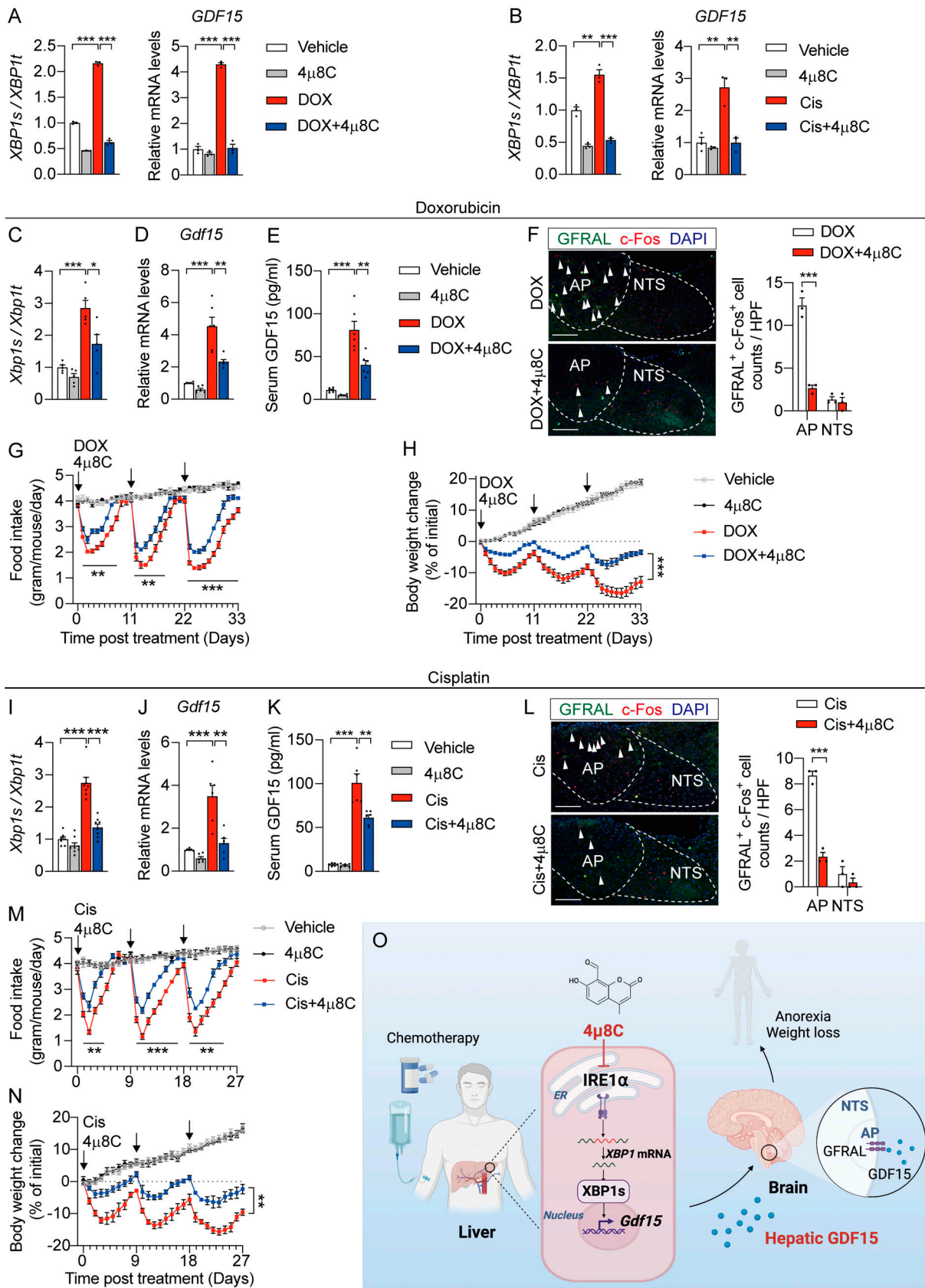


Figure 5. **Pharmacologic blocking of IRE1 α activity alleviates chemotherapy-induced anorexia and body weight loss via suppression of hepatic GDF15.** (A and B) XBP1 mRNA splicing and GDF15 mRNA levels in Huh7 cells treated with (A) Vehicle, 4 μ 8C (1 μ M), DOX (0.01 μ g/ml), or DOX+4 μ 8C or (B) Vehicle, 4 μ 8C (1 μ M), Cis (10 μ M), or Cis+4 μ 8C for 24 h. *n* = 3 per group. (C–H) Male C57BL/6 mice were treated with Vehicle, 4 μ 8C (3.3 mg per kg body weight,

i.p.), DOX (5 mg per kg body weight, i.p.), or the combination of DOX and 4 μ 8C at the indicated time points (black arrows) for three doses of treatment. **(C and D)** *Xbp1* mRNA splicing (C) and *Gdf15* mRNA levels (D) in liver samples from mice after the treatments. Veh., $n = 5$; 4 μ 8C, $n = 5$; DOX, $n = 5$; DOX+4 μ 8C, $n = 5$. **(E)** Circulating GDF15 protein levels in mice after the treatments. Veh., $n = 6$; 4 μ 8C, $n = 6$; DOX, $n = 6$; DOX+4 μ 8C, $n = 6$. **(F)** Representative images of immunofluorescence staining against c-Fos and GFRAL at the area AP and NTS of the murine brainstem (left). GFRAL⁺ c-Fos⁺ cells (indicated by arrowheads, left) per HPF were quantified (right). The frozen brainstem slides were from mice at 1 day after the final treatments. Scale bar, 100 μ m. **(G and H)** Daily food intake (G, Veh., $n = 4$; 4 μ 8C, $n = 4$; DOX, $n = 4$; DOX+4 μ 8C, $n = 4$) and body weight changes (H, Veh., $n = 6$; 4 μ 8C, $n = 6$; DOX, $n = 6$; DOX+4 μ 8C, $n = 6$) of mice following the indicated treatments. **(I–N)** C57BL/6 male mice were treated with three doses of Vehicle, 4 μ 8C (3.3 mg per kg body weight, i.p.), Cis (5 mg per kg body weight, i.p.), or the combination of Cis and 4 μ 8C at the indicated time points (black arrows). **(I and J)** *Xbp1* mRNA splicing (I, Veh., $n = 7$; 4 μ 8C, $n = 8$; Cis, $n = 8$; Cis+4 μ 8C, $n = 8$) and *Gdf15* mRNA levels (J, Veh., $n = 6$; 4 μ 8C, $n = 6$; Cis, $n = 6$; Cis+4 μ 8C, $n = 6$) in liver samples from mice after the treatments. **(K)** Circulating GDF15 protein levels in mice after the treatments. Veh., $n = 6$; 4 μ 8C, $n = 6$; Cis, $n = 6$; Cis+4 μ 8C, $n = 6$. **(L)** Representative images of immunofluorescence staining against c-Fos and GFRAL at the area AP and NTS of the murine brainstem (left). GFRAL⁺ c-Fos⁺ cells (indicated by arrowheads, left) per HPF were quantified (right). The frozen brainstem slides were from mice at 1 day after the final treatments. Scale bar, 100 μ m. **(M and N)** Daily food intake (M, Veh., $n = 3$; 4 μ 8C, $n = 3$; Cis, $n = 4$; Cis+4 μ 8C, $n = 4$) and body weight changes (N, Veh., $n = 6$; 4 μ 8C, $n = 6$; Cis, $n = 6$; Cis+4 μ 8C, $n = 6$) of mice following the treatments. **(O)** Proposed model: Hepatic IRE1 α -XBP1 signaling activated by chemo drugs regulates hepatic GDF15 expression and promotes chemotherapy-induced anorexia and body weight loss. Data are representative of three independent experiments (A and B) or two independent experiments (C–M) and presented as mean \pm SEM. * $P < 0.05$, ** $P < 0.01$, *** $P < 0.001$ by two-way ANOVA (A–E and I–K) or unpaired two-tailed Student's t test (F–H and L–N).

IRE1 α -XBP1 pathway leads to upregulation of *Gdf15* expression, and consequently, elevation of circulating GDF15 levels results in activation of GFRAL-expressing neurons. This liver–brain crosstalk in turn triggers anorexia and body weight loss. Moreover, pharmacologic inhibition of hepatic IRE1 α RNase activity offers a potential therapeutic approach for effectively alleviating these side effects of chemotherapy (Fig. 5 O). Hence, our findings have important translational implications not only for chemotherapy-associated adverse effects, but also for other GDF15-related wasting conditions.

Materials and methods

Animals

Adult wild-type male mice (C57BL/6J; 8 wk old) were obtained from Hangzhou Ziyuan Laboratory Animal Technology Co., Ltd. Liver-specific IRE1 α knockout (LKO, *Albumin-Cre; Ernl^{flox/flox}*) mice on the C57BL/6 background were generated by intercrossing the ER to nucleus signaling 1 (*Ernl*) floxed (*flox/flox*, *Ernl^{flox/flox}*) mice, in which the exon 2 of the *Ernl* allele was flanked by loxP sites, with the Albumin-Cre mice as described (Shao et al., 2014). The mice were generated at Hangzhou Ziyuan Laboratory Animal Technology Co., Ltd. and maintained at 23 \pm 3°C with a humidity of 35 \pm 5% under a 12-h dark–light cycle, with free access to water and food. Whole-body *Gdf15* gene knockout mice (*Gdf15^{KO}*, strain no. T011862) were obtained from GemPharmatech Co., Ltd. All animal experiments were performed according to protocols approved by the Institutional Animal Care and Use Committee at Zhejiang Academy of Traditional Chinese Medicine, Tongde Hospital of Zhejiang Province.

Mouse studies

For the evaluation of chemotherapy effects in healthy mice, 8-wk-old C57BL/6J male mice were randomized into indicated groups before the treatments, respectively. Chemotherapy agents were administered as described in the section Chemotherapy drugs.

For the inhibition of RNase activity of IRE1 α in vivo, 8-wk-old male C57BL/6J mice were randomized into the indicated groups and received the i.p. injection of IRE1 α inhibitor 4 μ 8C (3.3 mg/kg body weight, #S7272; Selleck) or DMSO (in 16% vol/vol Cremophor EL; Sigma-Aldrich) in combination with

chemotherapeutic drugs. These mice were administered for two additional doses of chemo drugs and 4 μ 8C at the indicated time. Additional solvents (double distilled water/saline+DMSO+Cre-mophor EL) in equal doses to the groups of DOX/Cis+4 μ 8C were i.p. injected into mice of control groups.

For silencing the expression of hepatic GDF15, 6-wk-old C57BL/6J male mice were tail-vein injected with AAV, which ectopically overexpress shRNA targeting at murine *Gdf15* mRNA (AAV-sh*Gdf15*-1) or control virus (AAV-shNC). 4 wk after the injection, animals were sacrificed for the evaluation of knock-down efficiency or administered with indicated chemotherapy agents for further analysis.

For the study of tumor-bearing mouse model, 8-wk-old male *flox/flox* or LKO mice received 5 \times 10⁵ Hepa1-6 cells by subcutaneous injection, respectively. The mice received the administration of DOX (5 mg per kg body weight) or vehicle at day 9 and 15 after the inoculation, respectively. Tumor growth was monitored daily following inoculation via measuring the tumor size three times per week using digital calipers. At day 7 after the inoculation, the palpable tumors were removed by surgery to mimic the clinical situation. For all the animal studies, body weight and food intake were determined around 09:00 in a day using a digital scale.

Chemotherapy drugs

DOX (#S1208) and PTX (#S1150) were purchased from Selleck. Cis was purchased from Sigma-Aldrich (#C2210000). The chemotherapy agents were delivered via intraperitoneal (i.p.) administration and dosed once: DOX (2 mg/ml in sterile water; 10 mg/kg), Cis (1 mg/ml in 0.9% saline; 10 mg/kg), and PTX (20 mg/ml in 66.6% Cremophor EL: ethanol in 0.9% saline; 10 mg/kg). For multiple chemotherapy dosing experiments, DOX (2 mg/ml in sterile water; 5 mg/kg) was administered on day 0, day 11, and day 22, and Cis (1 mg/ml in 0.9% saline; 5 mg/kg) was administered on day 0, day 9, and day 18, respectively. Doses for the chemotherapy agents were chosen in an attempt to induce ~10–30% weight loss (Breen et al., 2020) with minor modifications according to the experimental results.

AAV

pAAV-U6-shNC-EGFP, pAAV-U6-sh*Gdf15*-1-EGFP, and pAAV-U6-sh*Gdf15*-2-EGFP plasmids were constructed at GenePharma

Co. Ltd. The plasmids were packaged into AAV vector serotype DJ (AAV-DJ) by GenePharma utilizing standard plasmid transfection protocols. The silencing efficiency of pAAV-U6-shGdf15-1-EGFP and pAAV-U6-shGdf15-2-EGFP was evaluated in Hep1-6 cells and AAV-shGdf15-1 was chosen for the subsequent in vivo assays. AAVDJ-U6-shNC-EGFP (titer: 2.77×10^{12} vector genome [V.G]/ml) and AAVDJ-U6-shGdf15-1-EGFP (titer: 9.37×10^{12} V.G/ml) were diluted in PBS and administered at a dose of 1.0×10^{11} V.G/mouse via tail-vein injection (100 μ l in total volume). The target sequences for shRNAs against *Gdf15* mRNA are shown in Table S6.

RNA-seq analysis

Total RNA was isolated from freshly frozen liver tissues from the mice treated with chemotherapy agents ($n = 5$ individual mice per group) by TRIzol reagent (#T9424; Invitrogen). RNA library was prepared and sequenced by Berry Genomics. In brief, mRNA was purified from total RNA using polyT and then fragmented into 300–350 bp fragments, the first-strand cDNA was reverse-transcribed using fragmented RNA and dNTPs (dATP, dTTP, dCTP, and dGTP) and second-strand cDNA synthesis was subsequently performed. Remaining overhangs of double-strand cDNA were converted into blunt ends via exonuclease/polymerase activities. After adenylation of 3' ends of DNA fragments, sequencing adaptors were ligated to the cDNA and the library fragments were purified. The template was enriched by PCR, and the PCR product was purified to obtain the final library. After library preparation and pooling of different samples, the samples were subjected for Illumina sequencing.

The analysis of RNA-seq data was performed as previously described (Shan et al., 2021). Reads with phred quality scores <20 and <35 bp after trimming were removed from further analysis using trim-galore version 0.4.1. Quantity-filtered reads were then aligned to the mouse reference genome GRCm38 (mm10) using the HISAT (v 2.0.1) (Kim et al., 2015) aligner using default settings and marked duplicates using Sambamba version 0.6.6 (Tarasov et al., 2015). Aligned reads were quantified using “featurecount” (v1.4.6) (Liao et al., 2014) per gene ID against mouse Gencode version 20 (Frankish et al., 2019). Generation of normalized counts and analysis of differential gene expression was done using the R package EdgeR. The resulting P values were adjusted using the Benjamini and Hochberg approach for controlling the FDR. All RNA-seq data have been deposited to GEO (GSE235695).

Immunoblotting and antibodies

Immunoblotting assays were performed as previously described (Shan et al., 2017). In brief, cells or tissues were lysed by homogenization in radioimmunoprecipitation assay lysis buffer (150 mM NaCl, 1% NP-40, 0.5% sodium deoxycholate, 0.1% sodium dodecyl sulfate [SDS], 50 mM Tris-HCl, pH 7.4). Protein extracts were separated by SDS-polyacrylamide gel electrophoresis and then transferred onto a polyvinylidene difluoride membrane. Following overnight incubation with the indicated primary antibodies at 4°C, membranes were developed with Thermo Fisher Scientific's SuperSignal West Pico Chemiluminescent substrate or Millipore's Immobilon Western Chemiluminescent HRP substrate. The primary antibodies and diluted ratio include: anti-phospho-IRE1 α 1:1,000 (Ser724; #NB100-

2323; Novus Biologicals); anti-IRE1 α 1:1,000 (#3294; Cell Signaling Technology); anti-XBP1 1:1,000 (#ab220783; Abcam); anti- α -tubulin 1:1,000 (#3873; Cell Signaling Technology); anti-BiP 1:1,000 (#3182; Cell Signaling Technology); anti-ATF6 1:1,000 (#65880; Cell Signaling Technology); anti-phospho-eIF2 α 1:1,000 (#9721; Cell Signaling Technology); anti-eIF2 α 1:1,000 (#9722; Cell Signaling Technology); anti-ATF4 1:1,000 (#11815; Cell Signaling Technology); and anti-CHOP 1:1,000 (#2895; Cell Signaling Technology). Uncropped images of western blots presented in this study are in source data figures.

Immunofluorescence staining

Brain samples were collected from mice perfused and fixed with 4% PFA for 1 h. Tissues were then transferred to 30% sucrose in PBS at 4°C overnight. Fixed samples were O.C.T. embedded and cut into 5- μ m sections for staining. Sections were blocked with 3% normal horse serum in PBS at room temperature for 1 h and then incubated with anti-c-Fos (dilution: 1:300; #2250; Cell Signaling Technology) and anti-GFRAL (dilution: 1:100; #PA5-47769; Thermo Fisher Scientific) antibodies at 4°C overnight, followed by incubation with anti-rabbit-IgG-Alexa Fluor 555 (dilution: 1:500; #A32732; Thermo Fisher Scientific) and anti-sheep-IgG-Alexa Fluor 488 (dilution: 1:500; #ab150177; Abcam) antibodies for 2 h. Slides were then mounted with DAPI-containing antifade mounting medium (#BL739A; Biosharp), visualized under the LSM800 confocal laser scanning microscope, and analyzed with ZEN software (Zeiss).

Reverse transcription and quantitative PCR (RT-qPCR)

For RT-qPCR analysis, total RNA was isolated from liver tissues or cells by TRIzol reagent (#T9424; Invitrogen), and cDNA was synthesized using random hexamer primers (Thermo Fisher Scientific; #N8080127) and moloney murine leukemia virus reverse transcriptase (Thermo Fisher Scientific; #28025013) according to the manufacturer's instructions. Real-time PCR was performed using the SYBR Green PCR system (#4309155; Applied Biosystems). *Gapdh* was utilized as an internal control for calculation using the $\Delta\Delta$ -Ct method. All primers sequences used in this study are listed in Table S6.

Human specimens

For the evaluation of human circulating GDF15, plasma samples were obtained from healthy volunteers or individuals with cancers before and after receiving chemotherapy for the first time. Within the 37 individuals, 15 healthy volunteers were from our lab, 12 colon cancer patients were from the Hangzhou Third People's Hospital, and 10 breast cancer patients were from the First Affiliated Hospital, College of Medicine, Zhejiang University. The collection of peripheral blood samples from donors was approved by Medical Ethics Committee of Tongde Hospital of Zhejiang Province. All the individuals in this study were recruited with written informed consents. The clinical characteristics of all the patients are shown in Table S9.

GDF15 protein measurement

Circulating levels of GDF15 protein were respectively measured using the Mouse/Rat GDF15 ELISA kit (#DY6385; R&D) for

murine serum, or human GDF15 ELISA kit (#DGD150; R&D) for human plasma according to the manufacturer's instructions.

Cell culture

Huh7 cells and Hepa1-6 cells were generously provided by Dr. Daqian Xu (Zhejiang University). HEK293T cells (#CL-0005) were obtained from Procell Life Science & Technology Co., Ltd. Cells were cultured in Dulbecco's Modified Eagle's Medium (#C11995500BT; Gibco) supplemented with 10% fetal bovine serum (#164210; Procell) with the supplement of 1% penicillin/streptomycin (#15140122; Gibco). All cells were maintained at 37°C in a humidified atmosphere of 5% CO₂. Huh7 cells were seeded in 12-well plates and transfected with control vector or XBP1s-expressing vector using Lipofectamine 2000 (#11668027; Invitrogen) according to the manufacturer's instruction. 48 h after transfection, the cells were treated with chemotherapy agents and subsequently processed for further analysis.

Isolation of primary murine hepatocytes

Hepatocytes were isolated from mice at 8–12 wk of age as previously described (Liu et al., 2015). In brief, anesthetized mice were subjected to collagenase perfusion through the portal vein with 50 ml of perfusion buffer (Krebs Ringer buffer containing 3.6 mg/ml glucose, 1 M CaCl₂, and 5,000 U of collagenase I [Worthington]) at 37°C. The liver was aseptically removed to a sterile 10-cm cell culture dish with 20 ml of ice-cold perfusion buffer without collagenase. The excised liver was cut and hepatocytes were dispersed through aspiration using a large-bore pipette. After filtration through a 70-μm cell strainer (Thermo Fisher Scientific) into a 50-ml centrifuge tube and centrifugation at 50 × *g* for 2 min at 4°C, cells were then washed with cold Hepatocyte Wash Medium (Gibco) for three times and re-suspended in 15 ml of cold HepatoZYME-SFM (Gibco) medium supplemented with 2 mM L-glutamine, 10 units/ml penicillin, and 10 g/ml streptomycin. Cell viability was then determined by Trypan Blue staining, and hepatocytes were plated at 6 × 10⁵ cells/well in 6-well culture dishes or at 3 × 10⁵ cells/well in 12-well dishes that were pre-coated with collagen. Hepatocytes were cultured for 8 h before transfection with adenoviruses.

ChIP

ChIP was performed as previously described (Shan et al., 2020). Primary murine hepatocytes were prepared and transfected with adenoviruses expressing XBP1s-FLAG (Ad-XBP1s) or GFP (Ad-GFP). Cells were then cross-linked with 1% formaldehyde in PBS for 10 min at 37°C and quenched in 125 mM glycine in PBS for 5 min at 4°C. Cells were then lysed in Farnham lysis buffer (5 mM PIPES, pH 8.0, 85 mM KCl, 0.5% NP-40, 1 mM dithiothreitol [DTT], and protease inhibitor cocktail [#P8340; Sigma-Aldrich]). Crude nuclear pellets were collected by centrifugation before incubation in lysis buffer containing 5 mM Tris-HCl, pH 7.9, 1% SDS, 10 mM EDTA, 1 mM DTT, and protease inhibitor cocktail [#P8340; Sigma-Aldrich]. Chromatin fragmentation (~200–500 bp in length) was performed at 4°C by Bioruptor 300 using the setting of 10 cycles of 30 sec on and 60 sec off. Soluble chromatin was then diluted 1:10 with dilution buffer (20 mM Tris-HCl, pH 7.9, 0.5% Triton X-100, 2 mM EDTA, 150 mM NaCl,

1 mM DTT, and protease inhibitor cocktail [#P8340; Sigma-Aldrich]) and precleared using Protein G Sepharose 4 Fast Flow (#17-0618-01; GE Healthcare Biosciences) for 1 h at 4°C. Precleared samples were incubated with anti-XBP1 antibody (1:100 in dilution, #ab220783; Abcam) overnight at 4°C. Antibody-protein-DNA complexes were captured by incubation with Protein G Sepharose 4 Fast Flow (#17-0618-01; GE Healthcare Biosciences) at 4°C for 2 h. Immunoprecipitated material was consecutively washed with low-salt wash buffer (20 mM Tris-HCl, pH 7.9, 2 mM EDTA, 125 mM NaCl, 0.05% SDS, 1% Triton X-100, and protease inhibitor cocktail [#P8340; Sigma-Aldrich]), high-salt wash buffer (20 mM Tris-HCl, pH 7.9, 2 mM EDTA, 500 mM NaCl, 0.05% SDS, 1% Triton X-100, and protease inhibitor cocktail [#P8340; Sigma-Aldrich]), LiCl wash buffer (10 mM Tris-HCl, pH 7.9, 1 mM EDTA, 250 mM LiCl, 1% NP-40, 1% sodium deoxycholate, and protease inhibitor cocktail [#P8340; Sigma-Aldrich]), and 1× Tris-EDTA. After elution (100 mM NaHCO₃, 1% SDS), the immunoprecipitated material was digested with RNase (#11119915001; Roche) and proteinase K (#E00491; Thermo Fisher Scientific) prior to purification and concentration of the immunoprecipitated genomic DNA by ChIP DNA Clean & Concentrator Kit (#D5201; Zymo Research). ChIP-isolated DNA was subjected to qPCR (ChIP-qPCR). Sequences of the primers used in the assay are listed in Table S6.

Luciferase reporter assay

The *Gdf15* promoter-luciferase reporter plasmid and its mutant versions were constructed through a PCR-based cloning strategy. For luciferase activity analysis, HEK293T cells were co-transfected with the reporter plasmid, pCMV-XBP1s, and the pRL-TK-Renilla-luciferase plasmid. Luciferase activity was measured with Dual Luciferase Reporter Gene Assay Kit (#RG027; Beyotime Biotechnology) following the manufacturer's instructions, and Renilla luciferase activity was used for normalization.

For in vivo luciferase reporter assays, the luciferase reporter plasmids for mouse *Gdf15* promoter spanning the region from -1,028 to +1 were constructed in pGL3 (Promega) via a PCR-based cloning strategy. Reporter DNA constructs were introduced into livers of mice through hydrodynamic injection as described (Bell et al., 2007). Briefly, a DNA solution (12.5 mg/ml in sterile saline) was injected at 10% of volume/body weight through the tail vein within 10 sec, and mice were then administered with DOX or Cis 24 h later. Mice were imaged at 24 h after chemotherapeutic drug administration. For in vivo imaging, anesthetized mice were injected i.p. with 150 mg per kg D-Luciferin firefly-potassium salt (#40902ES03; Yeasen Biotechnology), and images were captured after 15 min by the IVIS Spectrum Imaging System and analyzed with Living Image software (PerkinElmer).

Statistical analysis

Statistical analysis was carried out as indicated in the figure legends. All data are presented as the mean ± SEM unless otherwise indicated in the figure legends. Data variance was examined by *F* test or Bartlett's test. The data meet the assumptions of the indicated statistical analysis. All tests were

performed as two sided. A P value <0.05 was considered statistically significant. All statistical analyses were performed using Microsoft Excel or GraphPad Prism 8.0 (GraphPad Software). All statistical information, including P values, samples sizes, and repetitions, is provided in Table S7.

Online supplemental material

Fig. S1 contains supporting data for chemo-induced anorexia and selective activation of the IRE1 α -XBP1 pathway in the liver. **Fig. S2** shows the necessity and sufficiency of GDF15 for chemo-induced anorexia. **Fig. S3** shows no impacts on liver homeostasis or chemo-induced liver damage upon hepatic IRE1 α ablation or pharmacological blocking of IRE1 α activity. Table S1 lists GSEA HALLMARK pathways enriched in DOX group. Table S2 lists GSEA HALLMARK pathways enriched in Cis group. Table S3 lists GSEA GO Biological Process enriched in DOX group. Table S4 lists GSEA MOTIF enriched in DOX group. Table S5 lists the overlapping upregulated 135 genes. Table S6 lists oligonucleotide primer sequences. Table S7 lists statistical data. Table S8 lists information of reagents and materials. Table S9 lists clinical characteristics.

Data availability

RNA-seq data have been deposited to Gene Expression Omnibus (accession GSE235695). All other data from this study have been shown in figures and online supplemental material.

Acknowledgments

We thank Daqian Xu (Zhejiang University, Hangzhou, China) for providing the Huh7 and Hepa1-6 cell lines. We thank Chao Bi from the Core Facilities, Zhejiang University School of Medicine for their technical support.

This work was supported by the grants from the National Key Research and Development Program of China (2022YFA1104102) to B. Shan, Leading Innovative and Entrepreneur Team Introduction Program of Zhejiang (2022R01002) to B. Shan, the National Natural Science Foundation of China (32371235, 81972674, 31900543, 82303369, 81972693, 82170891, 82270926, and 32241008) to Y. Wu, Y. Tang, W. Chen, M. Shao, and B. Shan, the Fundamental Research Funds for the Central Universities (226-2023-00061 and 226-2024-00024) to B. Shan, the Natural Science Funding of Zhejiang Province (LQ23H160003, LR20H160001) to Y. Tang and W. Chen, Zhejiang Provincial Program for the Cultivation of High-level Innovative Health Talents to Y. Wu and W. Chen, Shanghai Municipal Science and Technology Project (22140903200) to M. Shao, State Administration of Traditional Chinese Medicine Science and Technology Department-Zhejiang Provincial Administration of Traditional Chinese Medicine Co-construction of Key Laboratory (no. GZY-ZJ-SY-2402), and Institute Specific Foundation for Zhejiang Provincial Department of Science and Technology (YSZX2401).

Author contributions: Y. Tang, T. Yao, B. Shan, and Y. Wu designed the study and performed most of the experiments and analyzed the data. X. Tian, X. Xia, X. Huang, Z. Qin, L. Zhao, Y. Zhao, B. Diao, Y. Ping, X. Zheng, and T. Qian participated in collection and analysis of the data. Z. Shen collected and

provided the human samples used in this study. Y. Xu and H. Chen assisted some of the animal experiments. T. Ma, B. Zhou, S. Xu, Q. Zhou, Y. Liu, M. Shao, and W. Chen contributed reagents, technical support, and provided scientific insight and discussion. M. Shao, B. Shan, and Y. Wu conceptualized the study, interpreted the experiments, and wrote the manuscript. Y. Wu supervised the work. All authors contributed to the manuscript and approved the submitted version.

Disclosures: The authors declare no competing interests exist.

Submitted: 9 August 2023

Revised: 26 February 2024

Accepted: 2 April 2024

References

- Aapro, M., P. Ruffo, R. Panteri, S. Costa, and V. Piovesana. 2018. Oncologist perspectives on chemotherapy-induced nausea and vomiting (CINV) management and outcomes: A quantitative market research-based survey. *Cancer Rep.* 1:e1127. <https://doi.org/10.1002/cnr2.1127>
- Appierto, V., P. Tiberio, M.G. Villani, E. Cavadini, and F. Formelli. 2009. PLAB induction in fenretinide-induced apoptosis of ovarian cancer cells occurs via a ROS-dependent mechanism involving ER stress and JNK activation. *Carcinogenesis.* 30:824–831. <https://doi.org/10.1093/carcin/bgp067>
- Baek, S.J., J.S. Kim, J.B. Nixon, R.P. DiAugustine, and T.E. Eling. 2004. Expression of NAG-1, a transforming growth factor-beta superfamily member, by troglitazone requires the early growth response gene EGR-1. *J. Biol. Chem.* 279:6883–6892. <https://doi.org/10.1074/jbc.M305295200>
- Barreto, R., Y. Kitase, T. Matsumoto, F. Pin, K.C. Colston, K.E. Couch, T.M. O'Connell, M.E. Couch, L.F. Bonewald, and A. Bonetto. 2017. ACVR2B/Fc counteracts chemotherapy-induced loss of muscle and bone mass. *Sci. Rep.* 7:14470. <https://doi.org/10.1038/s41598-017-15040-1>
- Bell, J.B., K.M. Podetz-Pedersen, E.L. Aronovich, L.R. Belur, R.S. McIvor, and P.B. Hackett. 2007. Preferential delivery of the Sleeping Beauty transposon system to livers of mice by hydrodynamic injection. *Nat. Protoc.* 2:3153–3165. <https://doi.org/10.1038/nprot.2007.471>
- Bootcov, M.R., A.R. Bauskin, S.M. Valenzuela, A.G. Moore, M. Bansal, X.Y. He, H.P. Zhang, M. Donnellan, S. Mahler, K. Pryor, et al. 1997. MIC-1, a novel macrophage inhibitory cytokine, is a divergent member of the TGF-beta superfamily. *Proc. Natl. Acad. Sci. USA.* 94:11514–11519. <https://doi.org/10.1073/pnas.94.21.11514>
- Borner, T., E.D. Shaullson, M.Y. Ghidewon, A.B. Barnett, C.C. Horn, R.P. Doyle, H.J. Grill, M.R. Hayes, and B.C. De Jonghe. 2020a. GDF15 induces anorexia through nausea and emesis. *Cell Metab.* 31:351–362.e5. <https://doi.org/10.1016/j.cmet.2019.12.004>
- Borner, T., H.S. Wald, M.Y. Ghidewon, B. Zhang, Z. Wu, B.C. De Jonghe, D. Breen, and H.J. Grill. 2020b. GDF15 induces an aversive visceral malaise state that drives anorexia and weight loss. *Cell Rep.* 31:107543. <https://doi.org/10.1016/j.celrep.2020.107543>
- Breen, D.M., H. Kim, D. Bennett, R.A. Calle, S. Collins, R.M. Esquejo, T. He, S. Joaquim, A. Joyce, M. Lambert, et al. 2020. GDF-15 neutralization alleviates platinum-based chemotherapy-induced emesis, anorexia, and weight loss in mice and nonhuman primates. *Cell Metab.* 32:938–950.e6. <https://doi.org/10.1016/j.cmet.2020.10.023>
- Breit, S.N., D.A. Brown, and V.W. Tsai. 2021. The GDF15-GFRAL pathway in health and metabolic disease: Friend or Foe? *Annu. Rev. Physiol.* 83:127–151. <https://doi.org/10.1146/annurev-physiol-022020-045449>
- Chen, V.P., Y. Gao, L. Geng, and S. Brimijoin. 2017. Butyrylcholinesterase regulates central ghrelin signaling and has an impact on food intake and glucose homeostasis. *Int. J. Obes.* 41:1413–1419. <https://doi.org/10.1038/ijo.2017.123>
- Chung, H.K., D. Ryu, K.S. Kim, J.Y. Chang, Y.K. Kim, H.S. Yi, S.G. Kang, M.J. Choi, S.E. Lee, S.B. Jung, et al. 2017. Growth differentiation factor 15 is a myomittokine governing systemic energy homeostasis. *J. Cell Biol.* 216:149–165. <https://doi.org/10.1083/jcb.201607110>
- Coll, A.P., M. Chen, P. Taskar, D. Rimmington, S. Patel, J.A. Tadross, I. Cimino, M. Yang, P. Welsh, S. Virtue, et al. 2020. GDF15 mediates the effects of

- metformin on body weight and energy balance. *Nature*. 578:444–448. <https://doi.org/10.1038/s41586-019-1911-y>
- Cunningham, S.C., and I.E. Alexander. 2019. AAV-mediated gene delivery to the mouse liver. *Methods Mol. Biol.* 1937:213–219. https://doi.org/10.1007/978-1-4939-9065-8_12
- Dasari, S., and P.B. Tchounwou. 2014. Cisplatin in cancer therapy: Molecular mechanisms of action. *Eur. J. Pharmacol.* 740:364–378. <https://doi.org/10.1016/j.ejphar.2014.07.025>
- Day, E.A., R.J. Ford, B.K. Smith, P. Mohammadi-Shemirani, M.R. Morrow, R.M. Gutgesell, R. Lu, A.R. Raphenya, M. Kabiri, A.G. McArthur, et al. 2019. Metformin-induced increases in GDF15 are important for suppressing appetite and promoting weight loss. *Nat. Metab.* 1:1202–1208. <https://doi.org/10.1038/s42255-019-0146-4>
- Einhorn, L.H., B. Rapoport, R.M. Navari, J. Herrstedt, and M.J. Brames. 2017. 2016 updated MASCC/ESMO consensus recommendations: Prevention of nausea and vomiting following multiple-day chemotherapy, high-dose chemotherapy, and breakthrough nausea and vomiting. *Support. Care Cancer*. 25:303–308. <https://doi.org/10.1007/s00520-016-3449-y>
- Emmerson, P.J., F. Wang, Y. Du, Q. Liu, R.T. Pickard, M.D. Gonciarz, T. Coskun, M.J. Hamang, D.K. Sindelar, K.K. Ballman, et al. 2017. The metabolic effects of GDF15 are mediated by the orphan receptor GFRAL. *Nat. Med.* 23:1215–1219. <https://doi.org/10.1038/nm.4393>
- Frankish, A., M. Diekhans, A.M. Ferreira, R. Johnson, I. Jungreis, J. Loveland, J.M. Mudge, C. Sisu, J. Wright, J. Armstrong, et al. 2019. GENCODE reference annotation for the human and mouse genomes. *Nucleic Acids Res.* 47:D766–D773. <https://doi.org/10.1093/nar/gky955>
- Hesketh, P.J., K. Bohlke, and M.G. Kris. 2017. Antiemetics: American society of clinical oncology clinical practice guideline update summary. *J. Oncol. Pract.* 13:825–830. <https://doi.org/10.1200/JOP.2017.02.6351>
- Hetz, C., K. Zhang, and R.J. Kaufman. 2020. Mechanisms, regulation and functions of the unfolded protein response. *Nat. Rev. Mol. Cell Biol.* 21:421–438. <https://doi.org/10.1038/s41580-020-0250-z>
- Hill, C.M., T. Laeger, M. Dehner, D.C. Albarado, B. Clarke, D. Wanders, S.J. Burke, J.J. Collier, E. Qualls-Creekmore, S.M. Solon-Biet, et al. 2019. FGF21 signals protein status to the brain and adaptively regulates food choice and metabolism. *Cell Rep.* 27:2934–2947.e3. <https://doi.org/10.1016/j.celrep.2019.05.022>
- Hong, Y.S., H.R. Lee, S. Park, S.C. Lee, I.G. Hwang, B.B. Park, J. Lee, J.S. Ahn, M.J. Ahn, H.Y. Lim, and K. Park. 2006. Three-week schedule of irinotecan plus cisplatin in patients with previously untreated extensive-stage small-cell lung cancer. *Br. J. Cancer*. 95:1648–1652. <https://doi.org/10.1038/sj.bjc.6603500>
- Hsiao, E.C., L.G. Koniaris, T. Zimmers-Koniaris, S.M. Sebald, T.V. Huynh, and S.J. Lee. 2000. Characterization of growth-differentiation factor 15, a transforming growth factor beta superfamily member induced following liver injury. *Mol. Cell. Biol.* 20:3742–3751. <https://doi.org/10.1128/MCB.20.10.3742-3751.2000>
- Hsu, J.Y., S. Crawley, M. Chen, D.A. Ayupova, D.A. Lindhout, J. Higbee, A. Kutach, W. Joo, Z. Gao, D. Fu, et al. 2017. Non-homeostatic body weight regulation through a brainstem-restricted receptor for GDF15. *Nature*. 550:255–259. <https://doi.org/10.1038/nature24042>
- Huang, S., Y. Xing, and Y. Liu. 2019. Emerging roles for the ER stress sensor IRE1 α in metabolic regulation and disease. *J. Biol. Chem.* 294:18726–18741. <https://doi.org/10.1074/jbc.REV119.007036>
- Jensen-Cody, S.O., and M.J. Potthoff. 2021. Hepatokines and metabolism: Deciphering communication from the liver. *Mol. Metab.* 44:101138. <https://doi.org/10.1016/j.molmet.2020.101138>
- Jordan, M.A., and L. Wilson. 2004. Microtubules as a target for anticancer drugs. *Nat. Rev. Cancer*. 4:253–265. <https://doi.org/10.1038/nrc1317>
- Kelland, L. 2007. The resurgence of platinum-based cancer chemotherapy. *Nat. Rev. Cancer*. 7:573–584. <https://doi.org/10.1038/nrc2167>
- Kim, D., B. Langmead, and S.L. Salzberg. 2015. HISAT: A fast spliced aligner with low memory requirements. *Nat. Methods*. 12:357–360. <https://doi.org/10.1038/nmeth.3317>
- Liao, Y., G.K. Smyth, and W. Shi. 2014. featureCounts: An efficient general purpose program for assigning sequence reads to genomic features. *Bioinformatics*. 30:923–930. <https://doi.org/10.1093/bioinformatics/btt656>
- Liu, Y., M. Shao, Y. Wu, C. Yan, S. Jiang, J. Liu, J. Dai, L. Yang, J. Li, W. Jia, et al. 2015. Role for the endoplasmic reticulum stress sensor IRE1 α in liver regenerative responses. *J. Hepatol.* 62:590–598. <https://doi.org/10.1016/j.jhep.2014.10.022>
- Luan, H.H., A. Wang, B.K. Hilliard, F. Carvalho, C.E. Rosen, A.M. Ahasic, E.L. Herzog, I. Kang, M.A. Pisani, S. Yu, et al. 2019. GDF15 is an inflammation-induced central mediator of tissue tolerance. *Cell*. 178:1231–1244.e11. <https://doi.org/10.1016/j.cell.2019.07.033>
- Maida, A., A. Zota, K.A. Sjöberg, J. Schumacher, T.P. Sijmonsma, A. Pfenniger, M.M. Christensen, T. Gantert, J. Fuhrmeister, U. Rothermel, et al. 2016. A liver stress-endocrine nexus promotes metabolic integrity during dietary protein dilution. *J. Clin. Invest.* 126:3263–3278. <https://doi.org/10.1172/JCI85946>
- Marciniak, S.J., J.E. Chambers, and D. Ron. 2022. Pharmacological targeting of endoplasmic reticulum stress in disease. *Nat. Rev. Drug Discov.* 21:115–140. <https://doi.org/10.1038/s41573-021-00320-3>
- Matsubara, Y., H. Kiyohara, T. Teratani, Y. Mikami, and T. Kanai. 2022. Organ and brain crosstalk: The liver-brain axis in gastrointestinal, liver, and pancreatic diseases. *Neuropharmacology*. 205:108915. <https://doi.org/10.1016/j.neuropharm.2021.108915>
- McCullough, S.W. 2017. Chemotherapy-induced nausea and vomiting: Roles of pharmacists and formulary decision makers. *Am. J. Manag. Care*. 23:S266–S271.
- Minami, M., T. Endo, M. Hirafuji, N. Hamaue, Y. Liu, T. Hiroshige, M. Nemoto, H. Saito, and M. Yoshioka. 2003. Pharmacological aspects of anticancer drug-induced emesis with emphasis on serotonin release and vagal nerve activity. *Pharmacol. Ther.* 99:149–165. [https://doi.org/10.1016/S0163-7258\(03\)00057-3](https://doi.org/10.1016/S0163-7258(03)00057-3)
- Minotti, G., P. Menna, E. Salvatorelli, G. Cairo, and L. Gianni. 2004. Anthracyclines: Molecular advances and pharmacologic developments in antitumor activity and cardiotoxicity. *Pharmacol. Rev.* 56:185–229. <https://doi.org/10.1124/pr.56.2.6>
- Miyake, M., J. Zhang, A. Yasue, S. Hisanaga, K. Tsugawa, H. Sakaue, M. Oyadomari, H. Kiyonari, and S. Oyadomari. 2021. Integrated stress response regulates GDF15 secretion from adipocytes, preferentially suppresses appetite for a high-fat diet and improves obesity. *iScience*. 24:103448. <https://doi.org/10.1016/j.isci.2021.103448>
- Mullican, S.E., X. Lin-Schmidt, C.N. Chin, J.A. Chavez, J.L. Furman, A.A. Armstrong, S.C. Beck, V.J. South, T.Q. Dinh, T.D. Cash-Mason, et al. 2017. GFRAL is the receptor for GDF15 and the ligand promotes weight loss in mice and nonhuman primates. *Nat. Med.* 23:1150–1157. <https://doi.org/10.1038/nm.4392>
- Park, S.H., H.J. Choi, H. Yang, K.H. Do, J. Kim, H.H. Kim, H. Lee, C.G. Oh, D.W. Lee, and Y. Moon. 2012. Two in-and-out modulation strategies for endoplasmic reticulum stress-linked gene expression of pro-apoptotic macrophage-inhibitory cytokine 1. *J. Biol. Chem.* 287:19841–19855. <https://doi.org/10.1074/jbc.M111.330639>
- Patel, S., A. Alvarez-Guaita, A. Melvin, D. Rimmington, A. Dattilo, E.L. Miedzybrodzka, I. Cimino, A.C. Maurin, G.P. Roberts, C.L. Meek, et al. 2019. GDF15 provides an endocrine signal of nutritional stress in mice and humans. *Cell Metab.* 29:707–718.e8. <https://doi.org/10.1016/j.cmet.2018.12.016>
- Patel, S., A. Haider, A. Alvarez-Guaita, G. Bidault, J.S. El-Sayed Moustafa, E. Guiu-Jurado, J.A. Tadross, J. Warner, J. Harrison, S. Virtue, et al. 2022. Combined genetic deletion of GDF15 and FGF21 has modest effects on body weight, hepatic steatosis and insulin resistance in high fat fed mice. *Mol. Metab.* 65:101589. <https://doi.org/10.1016/j.molmet.2022.101589>
- Peterson, J.M., and D.C. Guttridge. 2008. Skeletal muscle diseases, inflammation, and NF- κ B signaling: Insights and opportunities for therapeutic intervention. *Int. Rev. Immunol.* 27:375–387. <https://doi.org/10.1080/08830180802302389>
- Potthoff, M.J., T. Inagaki, S. Satapati, X. Ding, T. He, R. Goetz, M. Mohammadi, B.N. Finck, D.J. Mangelsdorf, S.A. Kliewer, and S.C. Burgess. 2009. FGF21 induces PGC-1 α and regulates carbohydrate and fatty acid metabolism during the adaptive starvation response. *Proc. Natl. Acad. Sci. USA*. 106:10853–10858. <https://doi.org/10.1073/pnas.0904187106>
- Ramadori, G., and S. Cameron. 2010. Effects of systemic chemotherapy on the liver. *Ann. Hepatol.* 9:133–143. [https://doi.org/10.1016/S1665-2681\(19\)31651-5](https://doi.org/10.1016/S1665-2681(19)31651-5)
- Ruggiero, A., G. Trombatore, S. Triarico, R. Arena, P. Ferrara, M. Scalzone, F. Pierri, and R. Riccardi. 2013. Platinum compounds in children with cancer: Toxicity and clinical management. *Anticancer Drugs*. 24:1007–1019. <https://doi.org/10.1097/CAD.0b013e3283650bda>
- Shan, B., M. Shao, Q. Zhang, Y.A. An, L. Vishvanath, and R.K. Gupta. 2021. Cold-responsive adipocyte progenitors couple adrenergic signaling to immune cell activation to promote beige adipocyte accrual. *Genes Dev.* 35:1333–1338. <https://doi.org/10.1101/gad.348762.121>
- Shan, B., M. Shao, Q. Zhang, C. Hepler, V.A. Paschoal, S.D. Barnes, L. Vishvanath, Y.A. An, L. Jia, V.S. Malladi, et al. 2020. Perivascular mesenchymal cells control adipose-tissue macrophage accrual in obesity. *Nat. Metab.* 2:1332–1349. <https://doi.org/10.1038/s42255-020-00301-7>

- Shan, B., X. Wang, Y. Wu, C. Xu, Z. Xia, J. Dai, M. Shao, F. Zhao, S. He, L. Yang, et al. 2017. The metabolic ER stress sensor IRE1 α suppresses alternative activation of macrophages and impairs energy expenditure in obesity. *Nat. Immunol.* 18:519–529. <https://doi.org/10.1038/ni.3709>
- Shao, M., B. Shan, Y. Liu, Y. Deng, C. Yan, Y. Wu, T. Mao, Y. Qiu, Y. Zhou, S. Jiang, et al. 2014. Hepatic IRE1 α regulates fasting-induced metabolic adaptive programs through the XBP1s-PPAR α axis signalling. *Nat. Commun.* 5:3528. <https://doi.org/10.1038/ncomms4528>
- Suriben, R., M. Chen, J. Higbee, J. Oeffinger, R. Ventura, B. Li, K. Mondal, Z. Gao, D. Ayupova, P. Taskar, et al. 2020. Antibody-mediated inhibition of GDF15-GFRAL activity reverses cancer cachexia in mice. *Nat. Med.* 26:1264–1270. <https://doi.org/10.1038/s41591-020-0945-x>
- Tan, M., Y. Wang, K. Guan, and Y. Sun. 2000. PTGF-beta, a type beta transforming growth factor (TGF-beta) superfamily member, is a p53 target gene that inhibits tumor cell growth via TGF-beta signaling pathway. *Proc. Natl. Acad. Sci. USA.* 97:109–114. <https://doi.org/10.1073/pnas.97.1.109>
- Tao, G., J. Huang, B. Moorthy, C. Wang, M. Hu, S. Gao, and R. Ghose. 2020. Potential role of drug metabolizing enzymes in chemotherapy-induced gastrointestinal toxicity and hepatotoxicity. *Expert Opin. Drug Metab. Toxicol.* 16:1109–1124. <https://doi.org/10.1080/17425255.2020.1815705>
- Tarasov, A., A.J. Vilella, E. Cuppen, I.J. Nijman, and P. Prins. 2015. Sambamba: Fast processing of NGS alignment formats. *Bioinformatics.* 31:2032–2034. <https://doi.org/10.1093/bioinformatics/btv098>
- Tsai, V.W.W., Y. Husaini, A. Sainsbury, D.A. Brown, and S.N. Breit. 2018. The MIC-1/GDF15-GFRAL pathway in energy homeostasis: Implications for obesity, cachexia, and other associated diseases. *Cell Metab.* 28:353–368. <https://doi.org/10.1016/j.cmet.2018.07.018>
- von Holstein-Rathlou, S., L.D. BonDurant, L. Peltekian, M.C. Naber, T.C. Yin, K.E. Clafin, A.I. Urizar, A.N. Madsen, C. Ratner, B. Holst, et al. 2016. FGF21 mediates endocrine control of simple sugar intake and sweet taste preference by the liver. *Cell Metab.* 23:335–343. <https://doi.org/10.1016/j.cmet.2015.12.003>
- Walter, P., and D. Ron. 2011. The unfolded protein response: From stress pathway to homeostatic regulation. *Science.* 334:1081–1086. <https://doi.org/10.1126/science.1209038>
- Wang, D., E.A. Day, L.K. Townsend, D. Djordjevic, S.B. Jørgensen, and G.R. Steinberg. 2021. GDF15: Emerging biology and therapeutic applications for obesity and cardiometabolic disease. *Nat. Rev. Endocrinol.* 17:592–607. <https://doi.org/10.1038/s41574-021-00529-7>
- Wang, D., L.K. Townsend, G.J. DesOrmeaux, S.M. Frangos, B. Batchuluun, L. Dumont, R.E. Kuhre, E. Ahmadi, S. Hu, I.A. Rebalka, et al. 2023. GDF15 promotes weight loss by enhancing energy expenditure in muscle. *Nature.* 619:143–150. <https://doi.org/10.1038/s41586-023-06249-4>
- Winton, T., R. Livingston, D. Johnson, J. Rigas, M. Johnston, C. Butts, Y. Cormier, G. Goss, R. Incelet, E. Vallieres, et al. 2005. Vinorelbine plus cisplatin versus observation in resected non-small-cell lung cancer. *N. Engl. J. Med.* 352:2589–2597. <https://doi.org/10.1056/NEJMoa043623>
- Xie, B., A. Murali, A.M. Vandevender, J. Chen, A.G. Silva, F.M. Bello, B. Chuan, H. Bahudhanapati, I. Sipula, N. Dedousis, et al. 2022. Hepatocyte-derived GDF15 suppresses feeding and improves insulin sensitivity in obese mice. *iScience.* 25:105569. <https://doi.org/10.1016/j.isci.2022.105569>
- Yamamoto, K., H. Yoshida, K. Kokame, R.J. Kaufman, and K. Mori. 2004. Differential contributions of ATF6 and XBP1 to the activation of endoplasmic reticulum stress-responsive cis-acting elements ERSE, UPRE and ERSE-II. *J. Biochem.* 136:343–350. <https://doi.org/10.1093/jb/mvh122>
- Yang, H., S.H. Park, H.J. Choi, and Y. Moon. 2010. The integrated stress response-associated signals modulates intestinal tumor cell growth by NSAID-activated gene 1 (NAG-1/MIC-1/PTGF-beta). *Carcinogenesis.* 31:703–711. <https://doi.org/10.1093/carcin/bgq008>

Supplemental material

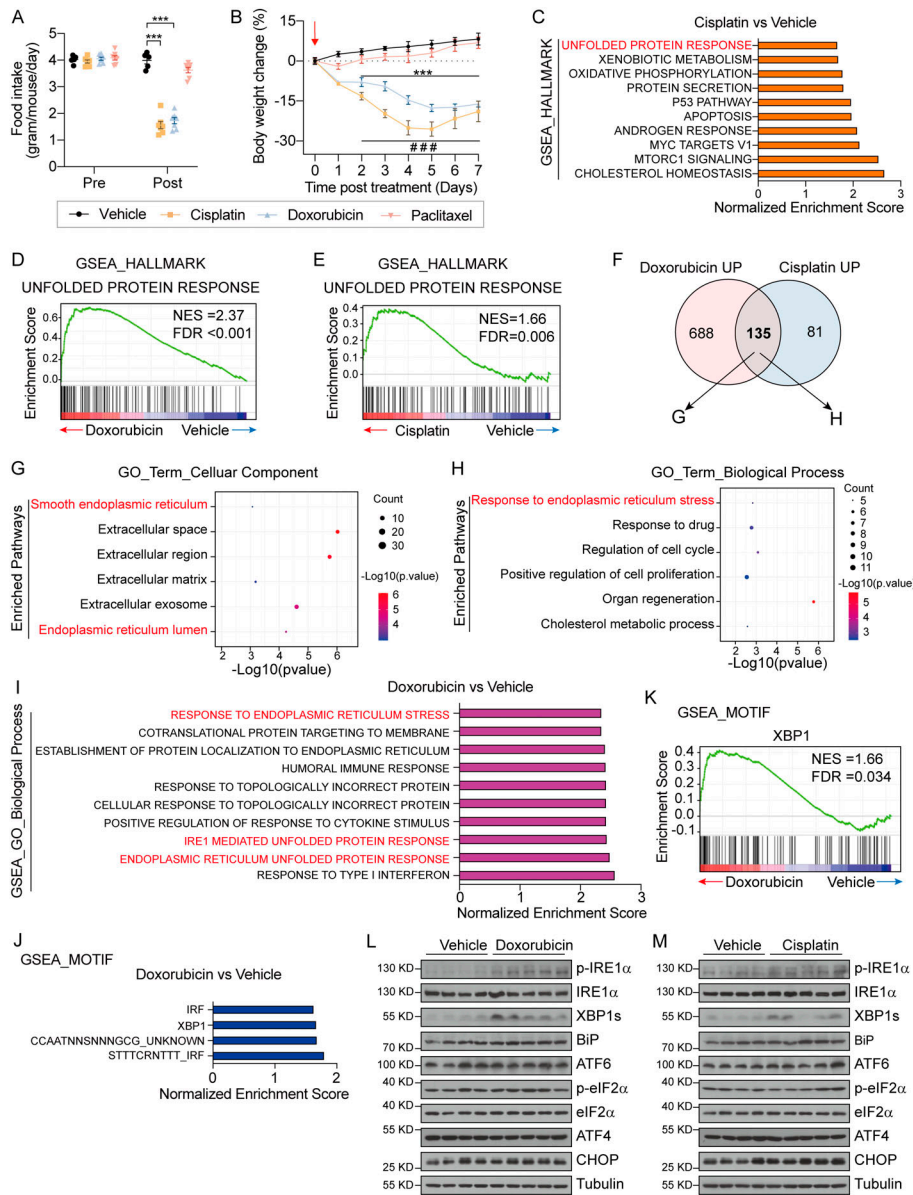


Figure S1. Chemotherapy with Cis and DOX causes anorexia and selective activation of the IRE1 α -XBP1 pathway in the liver. Related to Fig. 1. **(A and B)** Food intake (A) and body weight changes (B) of C57BL/6 mice treated with one dose of Vehicle (i.p.), DOX (10 mg per kg body weight, i.p.), Cis (10 mg per kg body weight, i.p.) or PTX (10 mg per kg body weight, i.p.) at 1 day. Vehicle, $n = 5$; DOX, $n = 7$; Cis, $n = 7$; PTX, $n = 7$. **(C)** Top 10 enriched HALLMARK pathways by the GSEA that are differentially regulated between liver samples from Vehicle- and Cis-treated mice. HALLMARK pathways are defined using the FPKM values of all the detected genes in livers from Cis-treated mice, and ranked according to the NES. **(D)** GSEA showing DOX-induced enrichment of the “unfolded protein response” gene signature in the liver (NES = 2.37 and FDR q -value < 0.001). The solid bars represent individual genes in the “unfolded protein response” gene set. **(E)** GSEA showing Cis-induced enrichment of the “unfolded protein response” gene signature in the liver (NES = 1.66 and FDR q -value = 0.006). The solid bars represent individual genes in “unfolded protein response” gene set. **(F)** Venn diagram showing the upregulated genes (compared to Vehicle treatment) that overlapped in liver samples from DOX- and Cis-treated mice. **(G and H)** GO analysis of the 135 overlapping genes in F. **(G)** Bubble plot of the top six enriched pathways by GO Term Biological Process analysis. **(H)** Bubble plot of the top six enriched pathways by GO Term Cellular Component analysis. The diameter of the circle is proportional to the number of DEGs enriched in the indicated pathways. The color of the circle represents the value of $-\log_{10}(P\text{-value})$. **(I)** The top 10 enriched pathways from GO Biological Process analysis by GSEA based on differentially regulated genes in the liver between Vehicle- and DOX-treated mice. The enriched pathways are defined using the FPKM values of all the detected genes in livers from DOX-treated mice, and ranked according to the NES. **(J)** The top four enriched motifs according to the MOTIF analysis by GSEA of the liver from Vehicle- and DOX-treated mice. The enriched motifs are defined using the FPKM values of all the detected genes in liver samples from DOX-treated mice and ranked according to the NES. **(K)** GSEA showing the enrichment of “XBP1” target gene signatures in liver samples from DOX-treated mice (NES = 1.66 and FDR q -value = 0.034). The solid bars represent individual genes in the “XBP1” gene set. **(L)** Western blot analysis of the indicated proteins in liver lysates from 8-wk-old mice treated with a single dose of DOX (10 mg per kg body weight, i.p.). Liver samples were collected 1 day after injection. Each sample represents an individual animal. **(M)** Western blot analysis of the indicated proteins in liver lysates from 8-wk-old mice treated with a single dose of Cis (10 mg per kg body weight, i.p.). Liver samples were collected 1 day after injection. Each sample represents an individual animal. Data are representative of two independent experiments and presented as mean \pm SEM. *** $P < 0.001$ (DOX versus Vehicle), ### $P < 0.001$ (Cis versus Vehicle) by unpaired two-tailed Student’s t test. Source data are available for this figure: SourceData FS1.

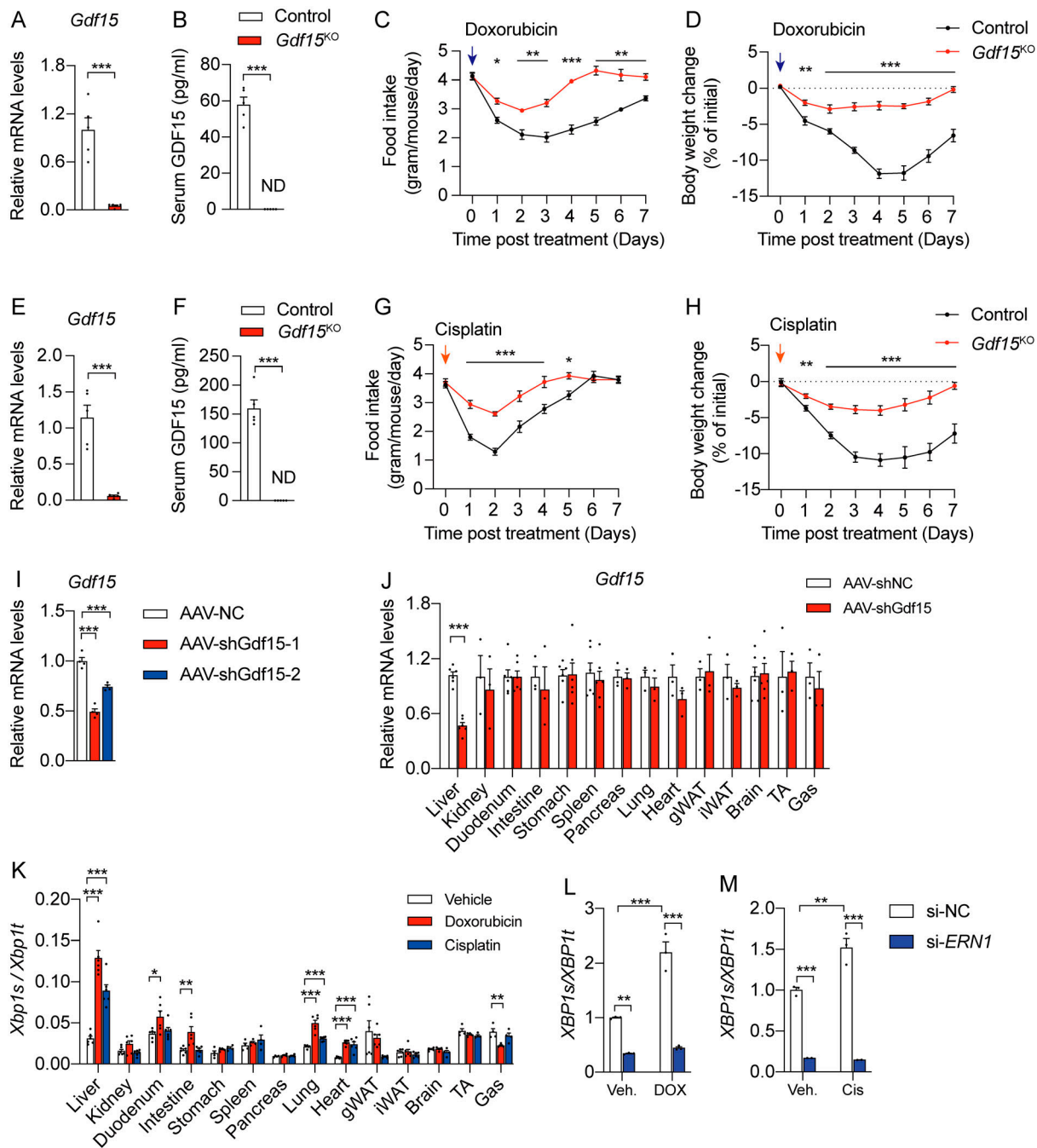


Figure S2. **Global *Gdf15* deficiency alleviates the chemotherapy-induced anorexia and body weight loss.** Related to Figs. 3 and 4. **(A–D)** *Gdf15*^{KO} (*n* = 5) and their littermates (Control, *n* = 5) were administered with one dose of Vehicle or DOX (5 mg per kg body weight, i.p.). **(A)** *Gdf15* mRNA levels in livers; **(B)** circulating GDF15 protein levels; **(C)** daily food intake; **(D)** body weight change. **(E–H)** *Gdf15*^{KO} (*n* = 5) and their littermates (Control, *n* = 5) were administered with one dose of Vehicle or Cis (5 mg per kg body weight, i.p.). **(E)** *Gdf15* mRNA levels in livers; **(F)** circulating GDF15 protein levels; **(G)** daily food intake; **(H)** body weight change. **(I)** mRNA levels of *Gdf15* in Hepa1-6 cells infected with AAV-shNC, AAV-shGdf15-1, or AAV-shGdf15-2 for 48 h (*n* = 4 per group). **(J)** mRNA levels of *Gdf15* in the indicated mouse tissues 4 wk after the injection of AAV-shNC (*n* = 3) or AAV-shGdf15 (*n* = 3). **(K)** *Xbp1* mRNA splicing in various tissues isolated from mice treated with Vehicle (*n* = 6), DOX (*n* = 6), or Cis (*n* = 6). Tissues were collected 1 day after injection. gWAT, gonadal white adipose tissue; iWAT, inguinal white adipose tissue; TA, tibialis anterior; Gas, gastrocnemius. **(L)** *XBP1* mRNA splicing in Huh7 cells transfected with control siRNA (si-NC) or siRNA against *ERN1* (si-*ERN1*) prior to treatment with Vehicle or DOX (0.01 μg/ml) for 48 h. *n* = 3 per group. **(M)** *XBP1* mRNA splicing in Huh7 cells transfected with control siRNA (si-NC) or siRNA against *ERN1* (si-*ERN1*) prior to treatment with Vehicle or Cis (10 μM) for 48 h. *n* = 3 per group. Data are representative of two independent experiments (A–H and G) or three independent experiments (I–K) and presented as mean ± SEM. **P* < 0.05, ***P* < 0.01, ****P* < 0.001 by unpaired two-tailed Student's *t* test (A–H) one-way ANOVA (I–K) and two-way ANOVA (L and M).

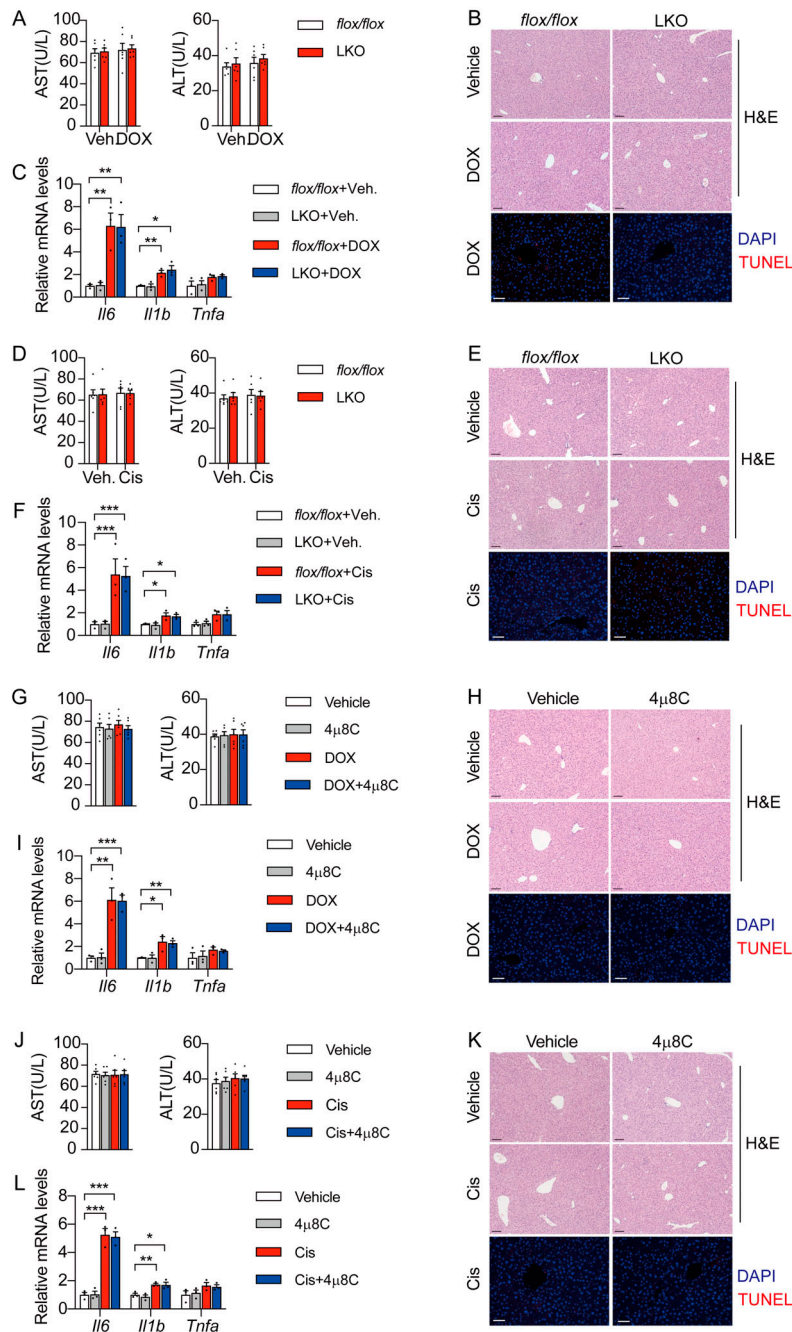


Figure S3. **Neither hepatic IRE1 α ablation nor pharmacological blocking of IRE1 α activity has impacts upon the homeostasis or chemo-induced damage of the liver.** (A–C) *flox/flox* (littermates) and LKO mice were i.p. injected with three doses of Vehicle (Veh.) and DOX (5 mg per kg body weight) at the time points shown in Fig. 2 B. (A) Serum aspartate aminotransferase (AST) and alanine aminotransferase (ALT) of the mice. *flox/flox*+Veh., *n* = 6; LKO+Veh., *n* = 6; *flox/flox*+DOX, *n* = 6; LKO+DOX, *n* = 6. (B) Representative H&E (scale bar, 100 μ m) and TUNEL (scale bar, 50 μ m) staining of liver sections. (C) mRNA levels of *Il6*, *Il1b*, and *Tnfa* genes in the liver samples. *flox/flox*+Veh., *n* = 3; LKO+Veh., *n* = 3; *flox/flox*+DOX, *n* = 3; LKO+DOX, *n* = 3. (D–F) *flox/flox* (littermates) and LKO mice were i.p. injected with three doses of Vehicle and Cis (5 mg per kg body weight) at the time points shown in Fig. 2 E. (D) Serum AST and ALT of the mice. *flox/flox*+Veh., *n* = 6; LKO+Veh., *n* = 6; *flox/flox*+Cis, *n* = 6; LKO+Cis, *n* = 6. (E) Representative H&E (scale bar, 100 μ m) and TUNEL (scale bar, 50 μ m) staining of liver sections. (F) mRNA levels of *Il6*, *Il1b*, and *Tnfa* in the liver samples. *flox/flox*+Veh., *n* = 3; LKO+Veh., *n* = 3; *flox/flox*+DOX, *n* = 3; LKO+DOX, *n* = 3. (G–I) C57BL/6 male mice were i.p. injected with Vehicle, 4 μ 8C (3.3 mg per kg body weight, i.p.), DOX (5 mg per kg body weight, i.p.), or the combination of DOX and 4 μ 8C for three doses at the time points as indicated in Fig. 5 G. (G) Serum AST and ALT of the mice. Veh., *n* = 6; 4 μ 8C, *n* = 6; DOX, *n* = 6; DOX+4 μ 8C, *n* = 6. (H) Representative H&E (scale bar, 100 μ m) and TUNEL (scale bar, 50 μ m) staining of the liver sections. (I) mRNA levels of *Il6*, *Il1b*, and *Tnfa* in the liver samples. Veh., *n* = 3; 4 μ 8C, *n* = 3; DOX, *n* = 3; DOX+4 μ 8C, *n* = 3. (J–L) C57BL/6 male mice were i.p. injected with Vehicle, 4 μ 8C (3.3 mg per kg body weight), Cis (5 mg per kg body weight), or the combination of Cis and 4 μ 8C for three doses at the time points as indicated in Fig. 5 M. (J) Serum AST and ALT of the mice. Veh., *n* = 6; 4 μ 8C, *n* = 6; Cis, *n* = 6; Cis+4 μ 8C, *n* = 6. (K) Representative H&E (scale bar, 100 μ m) and TUNEL (scale bar, 50 μ m) staining of the liver sections. (L) mRNA levels of *Il6*, *Il1b*, and *Tnfa* in the liver samples. Veh., *n* = 3; 4 μ 8C, *n* = 3; Cis, *n* = 3; Cis+4 μ 8C, *n* = 3. Data are representative of two independent experiments and presented as mean \pm SEM. **P* < 0.05, ***P* < 0.01, ****P* < 0.001 by two-way ANOVA (A, C, D, F, G, I, J, and L).

Provided online are nine tables. Table S1 shows gene sets enriched in the liver samples of DOX group relative to Vehicle group. Table S2 shows gene sets enriched in the liver samples of Cis-treated group relative to Vehicle group. Table S3 shows gene sets enriched in the liver samples of DOX group relative to Vehicle group. Table S4 shows gene sets enriched in the liver samples of DOX group relative to Vehicle group. Table S5 lists the overlapping 135 upregulated genes. Table S6 lists primer sequences used for qPCR. Table S7 shows statistical data (exact P values and sample/cohort sizes for each dataset in the study). Table S8 shows information of reagents and materials in this manuscript. Table S9 shows clinical characteristics of cancer patients.